Activity-dependent bidirectional regulation of terminal neuronal maturation in the adult hippocampus

2015

Yuki Imoto

TABLE OF CONTENTS

GENERAL INTRODUCTION

The hippocampus is one of the limbic structures and has a long-established role in learning and memory. In addition, it has become apparent that the hippocampus is an important regulator of emotion, and its dysfunction has been implicated in the pathophysiological basis of neuropsychiatric disorders, such as major depression and schizophrenia (Duman and Voleti, 2012; Decarolis and Eisch, 2010). The hippocampal structural connection is known as a trisynaptic circuit composed of the dentate gyrus (DG), and the CA1 and CA3 neurons (Figure 0-1). Granule cells (GCs) of the DG receive complex sensory information from the entorhinal cortex, and transfer the information to CA3 neurons via mossy fibers (MF), which are axons of GCs of the DG. The information received by CA3 neurons is transmitted to CA1 neurons through the Schaffer collateral pathway. Finally, the processed information is returned to the entorhinal cortex.

The DG is located at the starting point of the hippocampal trisynaptic circuit (Figure 0-1). In the mammalian DG, generation of GC neurons, which is called neurogenesis, is sustained throughout life due to proliferation of neural stem cells in the subgranular zone (SGZ) (Figure 0-2). Newborn GCs are integrated into granule cell layer (GCL), and finally become indistinguishable from pre-existing GCs within 2 months in rodents (Duan et al., 2008; Zhao et al., 2008). The continual supply of GCs is considered to be important for maintaining or reinforcing functions of the DG, although actual contribution of adult neurogenesis to neural functions has been still debated, because the number of additional newborn neurons would represent only a few percent of the total GC number (Ninkovic et al., 2007).

The principal cells of the DG are mature GCs. Given the high occupancy of mature GCs in the DG, functional modulation in mature GCs would have a great impact on hippocampal functions. Recent studies indicated that the maturation state of GCs may be modified even after they are completely maturated. Chronic treatment with selective serotonin reuptake inhibitor (SSRI) can reverse the established matured state of GCs to the late immature-like state in the adult mouse DG, which is called “dematuration” (Kobayashi et al., 2010). Dematured neurons show marked changes in physiological and functional properties, including expression of mature markers, neural excitability, and stimulus-induced responsibility (Figure 0-2). Furthermore, several studies have demonstrated that marked defects in the terminal maturation of GCs in the DG can be seen in animal models of neuropsychiatric disorders (Ohira et al., 2013; Takao et al., 2013; Yamasaki et al., 2008). It should be noted that, in Schnurri-2

knockout mice, which show molecular and behavioral phenotypes related to schizophrenia as well as the immaturity of GCs, expression of the mature GC markers is comparable to that of wild-type mice during early postnatal development, but starts to decrease toward adulthood before getting a fully matured level (Takao et al., 2013), suggesting that the final step of GC maturation is regulated by a dematuration-like process. However, the regulatory mechanism underlying the GC dematuration remains largely unknown. In addition, it has been reported that the dematured GC phenotype is observed concomitantly with enhanced adult neurogenesis in the DG (Takao et al., 2013; Yamasaki et al., 2008), although it is also unclear whether there is a relationship between the two phenomena.

In the present study, I set out to reveal the regulatory mechanism underlying GC dematuration and address whether there is a relationship between GC dematuration and adult neurogenesis. I found that enhanced neural activation induces dematuration of GCs (Chapter 1), and that dematuration and rematuration of GCs are bidirectionally regulated by glutamatergic excitation and GABAergic inhibition, respectively (Chapter 2). Finally, I found that progression of GC dematuration and enhancement of adult neurogenesis are closely associated (Chapter 3).

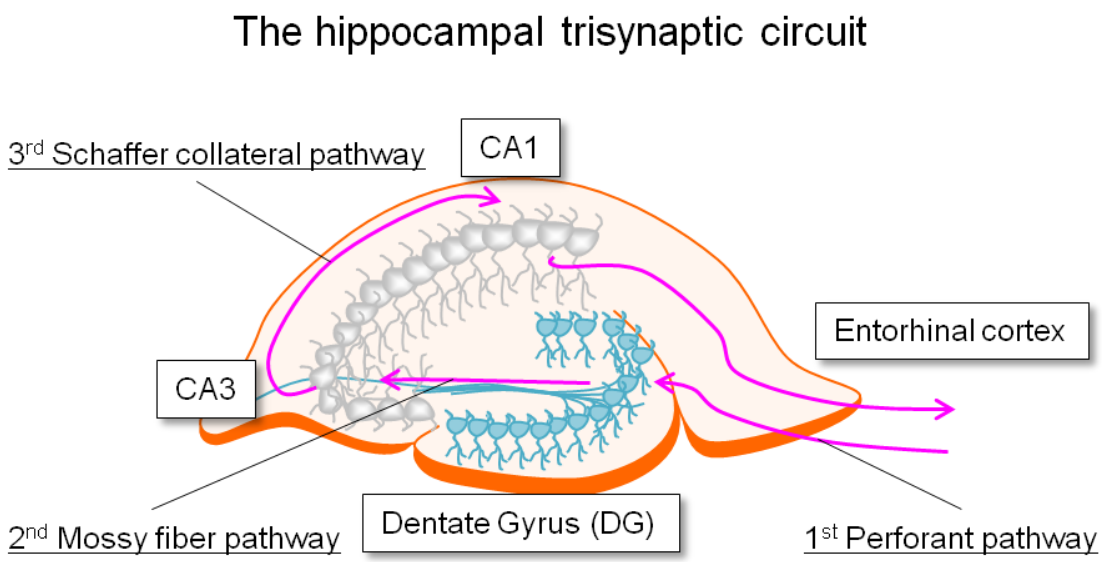

Figure 0-1. Model of the hippocampal trisynaptic circuit. Sensory information transmitted from the entorhinal cortex is processed in the following 3 pathways. 1st: Perforant pathway from the entorhinal cortex to the dentate gyrus (DG). 2nd: Mossy fiber pathway from the DG to CA3 neurons. 3rd: Schaffer collateral pathway from CA3 to CA1 neurons. The DG is located at the starting point of this circuit.

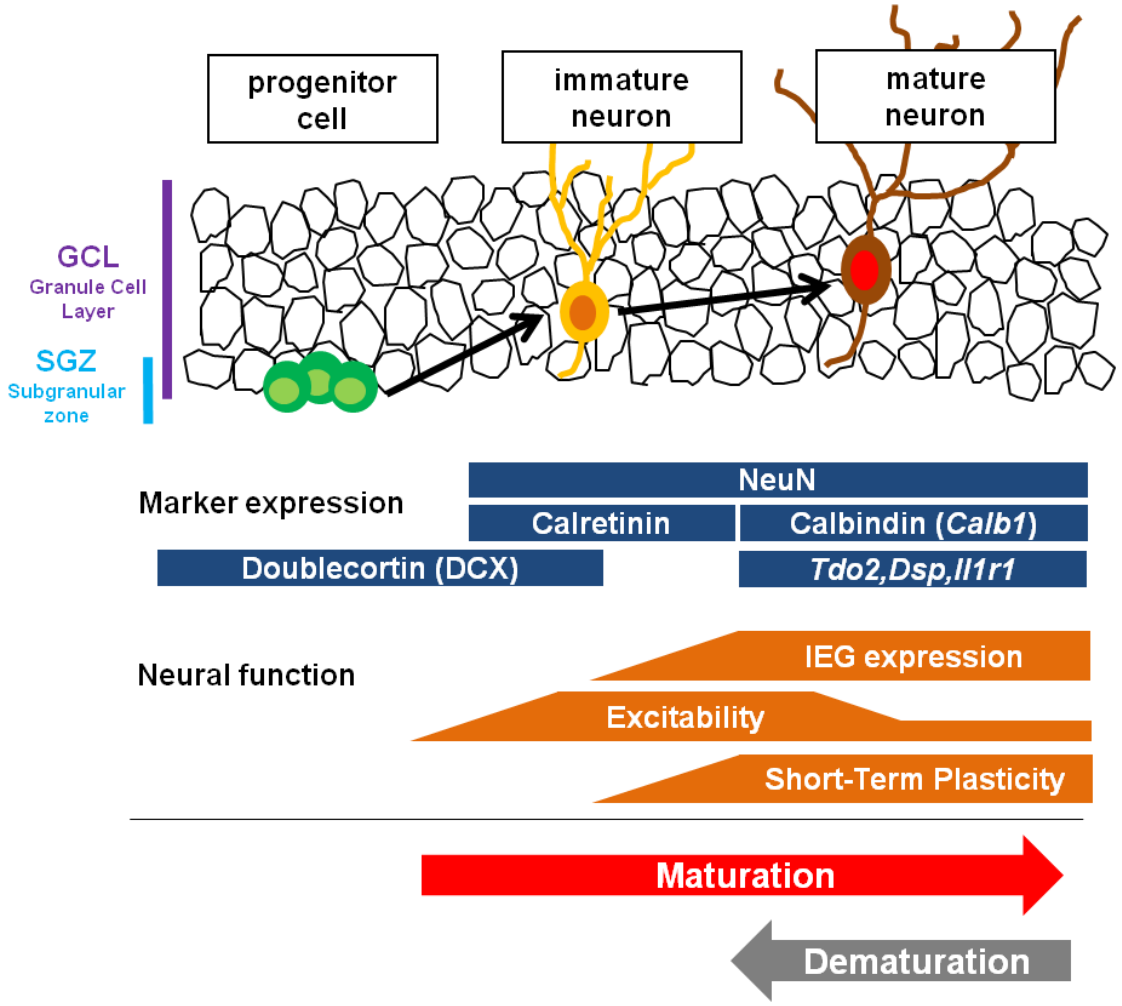

Figure 0-2. Maturation and dematuration models of GCs. Developmental stages of GCs in the DG can be identified by expression of stage markers and neural functions. IEG: immediate early genes, *Tdo2*: tryptophan 2,3-dioxygenase, *Dsp*: desmoplakin, *Il1r1*; interleukin 1 receptor type 1.

ABBREVIATIONS

ActD	actinomycin D
APV	D-(-)-2-amino-5-phosphonopentanoic acid
BDNF	brain-derived neurotrophic factor
BrdU	5-bromodeoxyuridine
CA	*cornu ammonis*
cDNA	complementary deoxyribonucleic acid
CNT	control
CNQX	6-cyano-7-nitroquinoxaline-2,3-dione
CPP	3-(2-carboxypiperazin-4-yl)propyl-1-phosphonic acid
CREB	cAMP response element binding protein
DAB	3,3'-diaminobenzidine
D-AP5	D-(-)-2-amino-5-phosphonopentanoic acid
DCG- IV	(2S,2'R,3'R)-2-(2',3'-dicarboxycyclopropyl)glycine
DCX	doublecortin
DG	dentate gyrus
DIG	digoxigenin
DMSO	dimethyl sulfoxide
ECS	electroconvulsive stimulation
ECT	electroconvulsive therapy
E/I	excitation/inhibition
EPSC	excitatory postsynaptic current
EPSP	excitatory postsynaptic potential
ERK	extracellular signal-regulated kinase
FLX	Fluoxetine
GABA	γ-aminobutyric acid
GC	granule cell
GCL	granule cell layer

ICV	intracerebroventricularly
IEG	immediate early gene
IR	immunoreactivity
IP	intraperitoneally
IPSC	inhibitory postsynaptic current
MAPK	mitogen-activated protein kinase
MF	mossy fiber
ML	molecular layer
MPP	medial perforant path
NMDA	N-methyl-D-aspartate
NMDAR	N-methyl-D-aspartate receptor
NPY	neuropeptide Y
mRNA	messenger RNA
PCR	polymerase chain reaction
PFA	Paraformaldehyde
RNA	ribonucleic acid
ROI	region of interest
RT-qPCR	semi-quantitative real-time PCR
SDS-PAGE	sodium dodecyl sulfate-polyacrylamide gel electrophoresis
SGZ	subgranular zone
SSRI	selective serotonin reuptake inhibitor
WT	wild-type
α-CaMKII	α-calcium/calmodulin-dependent protein kinase II
5,7-DHT	5,7-dihydroxytryptamine
5-HT	Serotonin
5-HT4R KO	5-HT_4 receptor knockout
5-HIAA	5-hydroxyindoleacetic acid

Chapter 1: Neural activation reverses mature phenotypes of granule cells in the dentate gyrus of the hippocampus

ABSTRACT

The maturity of granule cells (GCs) in the dentate gyrus (DG) would not be stable. It has been reported that chronic treatment of mice with selective serotonin reuptake inhibitor (SSRI) transforms the maturation state of GCs into an immature-like state, which is called “dematuration”. However, the regulatory mechanism underlying the terminal maturation of GCs remains largely unknown. In this chapter, I aimed at revealing the role of neural activity in regulating the terminal GC maturation. By neural activation with repeated electroconvulsive stimulation (ECS), mature GCs exhibited immature-like phenotypes, including reduced gene expression of mature GC markers, increased somatic excitability, and attenuated activity-dependent synaptic facilitation of the mossy fiber (MF) synapse. I found that the whole transcriptome profile of the DG after repeated ECS was strongly correlated with that of the SSRI-treated DG. In addition, I also showed that few times of ECS rapidly induces dematuration of mature GCs, and that repeated ECS stabilizes the dematured state. These results demonstrate that enhanced neural activation triggers dematuration of GCs, and repetitive neural activation converts the dematured state of GCs from a transient to a long-lasting form.

INTRODUCTION

Proper maturation of hippocampal neurons is crucial for functional integrity of the hippocampus. Developing granule cells (GCs) in the dentate gyrus (DG) show dramatic changes in the gene expression profile, morphology, and physiological functions (Duan et al., 2008; Zhao et al., 2008). In rodents, the full maturation of GCs is achieved in 6-7 weeks after the cell birth (Duan et al., 2008; Zhao et al., 2008), and the latter few weeks are devoted for establishing the functional maturity, including stimulus-dependent induction of immediate early genes (IEGs), synaptic plasticity, and synaptic excitation/inhibition balance in GCs (Duan et al., 2008, Kobayashi et al., 2010; Zhao et al., 2008).

Recent studies suggested that the maturity of GCs is not stable. For example, SSRI treatment reverses the mature state of GCs to the late immature stage even in the adult mice, which is called “dematuration” (Kobayashi et al., 2010). Defects in GC maturation have also been reported for several lines of mutant mice with abnormal behaviors associated with symptoms of schizophrenia and related neuropsychiatric disorders (Ohira et al., 2013; Takao et al., 2013; Yamasaki et al., 2008). These studies suggest that alteration of mature stages of GCs may underlie cellular mechanisms of antidepressants and/or be implicated in the basis of other types of neuropsychiatric disorders. Therefore, elucidating regulatory mechanisms underlying the terminal maturation of GCs would make contributions to understanding the molecular basis of neuropsychiatric disorders and developing novel approach to treat these diseases.

It has been generally believed that neural activity is known to regulate development of the nervous system. Although it has been reported that neural activity or excitation promotes structural and functional maturation of immature GCs (Overstreet-Wadiche et al., 2006; Ge et al., 2006; Piatti et al., 2011; Zhao et al., 2012), the facilitatory effects of the neural activity on GC maturation are typically observed at the early maturational stage. It remains largely unknown how neural activity modulates the late or terminal stage of GC maturation. In this chapter, I set out to reveal the role of neural activity in regulating the terminal neuronal maturation of GCs. To this end, I chose electroconvulsive stimulation (ECS) as excitatory stimulation. ECS is known to a model of electroconvulsive therapy, which is an effective and fast-acting treatment for depression, and robustly activate excitatory glutamatergic signaling in the DG of hippocampus (Ma et al., 2009; Stewart and Reid, 1994). In this chapter, I demonstrated that enhanced neural activation by ECS reverses the terminal maturation of hippocampal GCs.

RESULTS

Downregulation of mature granule cell markers by brief electrical stimulation

The matured state of GCs is characterized by several distinct molecular and physiological features (Duan et al., 2008; Zhao et al., 2008) (Figure 0-2). I first examined the gene expression of calbindin (*Calb1*), a marker for terminal maturation of GCs and found that single ECS strongly reduced *Calb1* expression in a DG-specific manner (Figure 1-1A). Single ECS reduced the expression of *Calb1* and tryptophan 2,3-dioxygenase (*Tdo2*), another mature GC marker, to essentially the same extent as repeated ECS (11 times over 3 weeks) at 6 h after the stimulation (Figure 1-1B). While *Calb1* and *Tdo2* expression levels returned toward the control level in 24 h after single ECS, they were continually downregulated at least for 14 days after repeated ECS (Figures 1-1C and 1-1D). The gene expression of other mature GC markers, desmoplakin (*Dsp*) and interleukin-1 receptor type 1 (*Il1r1*), was also reduced after single ECS (Figures 1-1E and 1-1F), although reduction in their expression after single ECS was slower than that of *Calb1* and *Tdo2*. The long-lasting reduction in the *Dsp* and *Il1r1* expression was also observed after 11 times of ECS. These results demonstrate that neural activation induces rapid downregulation of markers for GC terminal maturation and that repeated stimuli stabilize the downregulated state.

I also confirmed the reduction in the calbindin expression after repeated ECS at the protein level (Tonder et al., 1994) (Figures 1-2A, 1-2B and 1-2C). In contrast, the same treatment did not affect expression of a neuronal marker, NeuN (Figure 1-2C). In the subgranular zone (SGZ) of the DG, the expression of doublecortin and calretinin, markers for early immature GCs, was enhanced by repeated ECS probably due to increased adult neurogenesis. However, the majority of the NeuN-positive or calbindin-negative GCs in the DG did not express these markers after ECS (Figure 1-2C), suggesting that ECS-treated GCs are in an intermediate or late immature state lacking calretinin and calbindin expression (Brandt et al., 2003). The rapid downregulation of the mature GC markers excludes a possibility that mature GCs are largely replaced by newly generated young neurons. Thus, these results suggest that ECS changes the phenotype of mature GCs to that of immature GCs at the late immature stage.

Chronic SSRI treatment can reverse the state of GC maturation in adult mouse DG (Kobayashi et al., 2010, 2011, 2013). The comprehensive gene expression analysis revealed a striking similarity in the gene expression profiles between chronic SSRI- and repeated ECS-treated DG (Figure 1-3A). Among the genes that exhibited more than 2-fold changes by either ECS or SSRI treatment, 199 genes were changed in common

(Figure 1-3B). Functional gene ontology classification revealed an extremely high association of the genes significantly changed by both of the treatments with neuronal cell growth and development (Figure 1-3C). These results further support an idea that ECS changes the GC phenotypes from a mature to immature state.

Granule cells exhibit immature-like functional properties after electrical stimulation

I next performed a series of experiments to evaluate the state of the functional maturity of GCs after ECS. To this end, stimulus-induced expression of immediate early genes (IEGs), an index of the maturity of activity-dependent neuronal responsiveness *in vivo* (Jessberger and Kempermann, 2003; Zhao et al., 2008), was examined after single and repeated ECS. In agreement with a previous report (Hsieh et al., 1998), single ECS induced robust expression of the IEG c-fos in the majority of GCs (Figures 1-4A and 1-4B). This c-fos expression in GCs was strongly suppressed after repeated ECS (Figures 1-4A and 1-4B). The expression of other IEGs (*Gadd45b, Nr4a1, Arc,* and *Egr1*) was similarly attenuated after repeated ECS (Figure 1-4C). Thus, the mature responsiveness of GCs was suppressed during the course of repeated ECS treatments.

Next, electrophysiological properties of ECS-treated GCs were examined. Immature GCs show higher somatic excitability, higher input resistance, and more depolarized resting membrane potentials than mature GCs (Ambrogini et al., 2004). Repeated ECS increased somatic excitability of GCs and reduced resting membrane potentials, but had no significant effect on input resistance (Figures 1-5A and 1-5B).

Presynaptic characteristics at the synapse between the GC axon mossy fiber (MF) and a CA3 pyramidal cell can be a good physiological index of the functional maturity of GCs (Kobayashi et al., 2010). The mature MF synapse exhibits strong frequency facilitation, a form of presynaptic short-term plasticity, and the magnitude of MF frequency facilitation well correlates with the expression level of the mature GC marker *Calb1* (Kobayashi et al., 2010). To further characterize the functional maturity of ECS-treated GCs, the MF-CA3 synaptic transmission was analyzed. Repeated ECS reduced the frequency facilitation of MF excitatory postsynaptic potentials (EPSPs) to the juvenile level, but had no significant effect on the basal synaptic efficacy (Figures 1-6A and 1-6B). While 2 or 3 times of ECS had highly significant effects on frequency facilitation at 24 h after ECS (Figure 1-6C), the magnitude of facilitation completely returned to the control level in 14 days (Figure 1-6D). Repeated ECS caused a long-term reduction in frequency facilitation lasting more than 28 days (Figure 1-6D). Taken together, these results strongly suggest that the neuronal activation by ECS rapidly initiates dematuration of GCs. The rapidly induced dematuration is not stable,

and repeated ECS can convert the transient demature state into a long-lasting form and stabilize the state of GC maturation at the late immature stage (Figure 1-7).

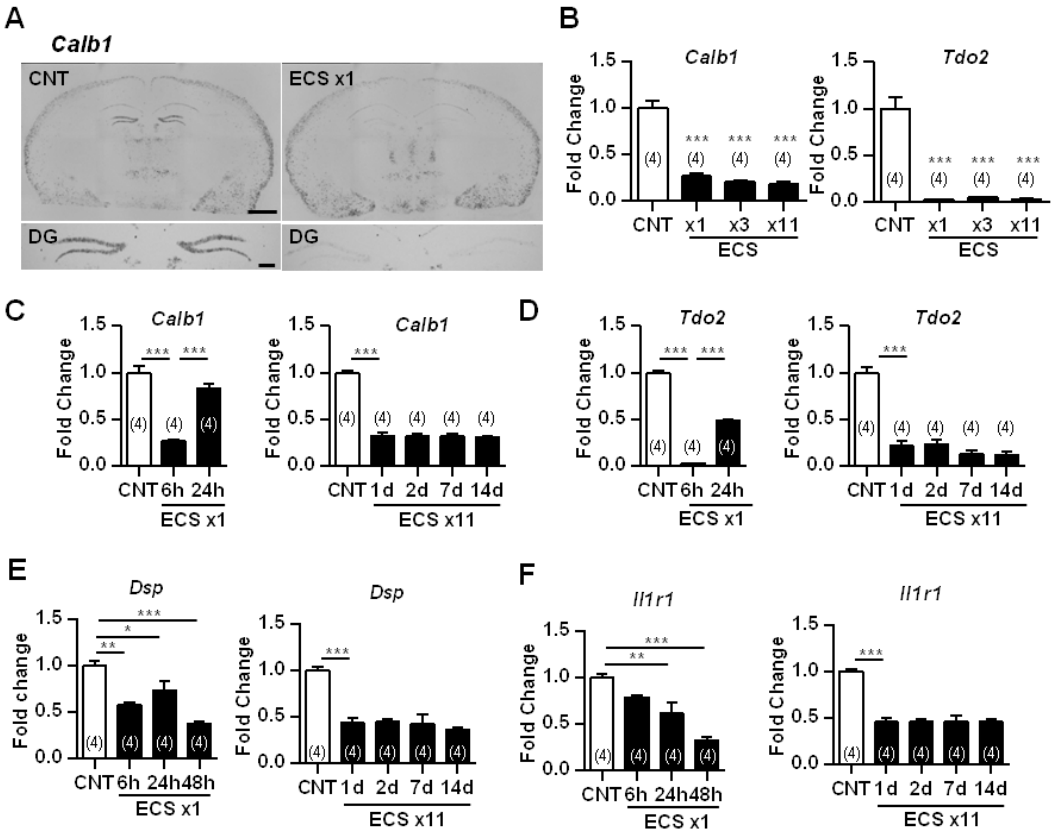

Figure 1-1. Reduction in gene expression of mature GC markers after ECS. (**A**) Representative images of *in situ* hybridization of *Calb1* at 6 h after single ECS or sham control treatment (CNT). Scale bar, upper 1 mm, lower 200 μm. (**B**) The relative expression of *Calb1* and *Tdo2* at 6 h after the indicated number of ECS (*** P < 0.001, Dunnett's test following one-way ANOVA). (**C, D**) The relative expression of *Calb1* and *Tdo2* at indicated time intervals after the last ECS (*** P < 0.001, Tukey's test following one-way ANOVA). (**E, F**) The relative expression of *Dsp* and *Il1r1* at indicated time intervals after ECS (* P < 0.05, ** P < 0.01, *** P < 0.001, Tukey's test following one-way ANOVA). The *n* numbers are given in parentheses. Data are presented as means ± SEM.

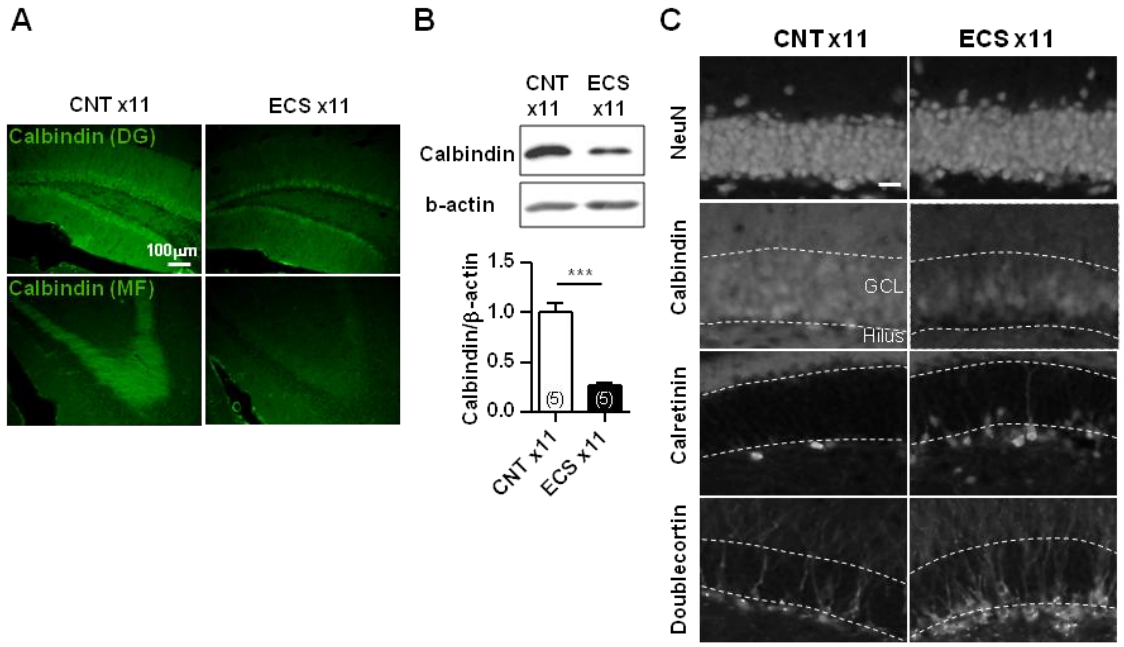

Figure 1-2. Alteration in the protein levels of GC stage markers in DG after ECS. (**A**) Representative images of immunoreactivity for calbindin D-28K in DG and MF at 24 h after 11 times of ECS. GCL: granule cell layer. MF: mossy fiber. Scale bar, 100 μm. (**B**) Immunoblot analysis of calbindin D-28K in DG (*** $P < 0.001$). The *n* numbers are given in parentheses. Data are presented as means ± SEM. (**E**) Representative images of immunoreactivity for NeuN, calbindin, calretinin, and doublecortin in DG at 24 h after 11 times of ECS. GCL: granule cell layer. Scale bar, 20 μm.

A

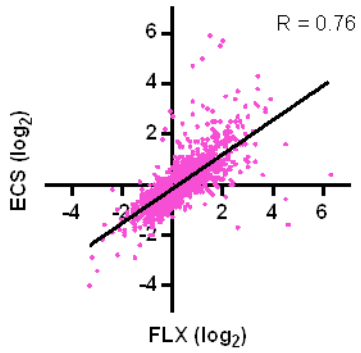

B

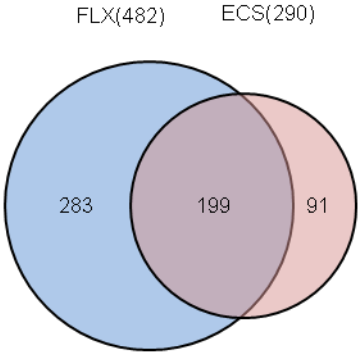

C

Gene ontology analysis

FLX and ECS

GO Term	Gene Number	P-Value
Behavior (GO:0007610)	15	0.000015
Regulation of cell growth (GO:0001558)	8	0.000017
Regulation of growth (GO:0040008)	12	0.000018
Regulation of cell development (GO:0060284)	9	0.000087
Regulation of neurogenesis (GO:0050767)	8	0.000175
Regulation of nervous system development (GO:0051960)	8	0.000354
Regulation of cell-substrate adhesion (GO:0010810)	5	0.000427
Neuropeptide signaling pathway (GO:0007218)	6	0.000648
Negative regulation of cell proliferation (GO:0008285)	9	0.000877

FLX only

GO Term	Gene Number	P-Value
Negative regulation of cell proliferation (GO:0008285)	14	0.000005
Regulation of cell proliferation (GO:0042127)	20	0.000051

ECS only

GO Term	Gene Number	P-Value
None	-	-

Figure 1-3. Correlation of gene expression changes in the DG between repeated ECS and chronic SSRI treatments. (**A**) Scatter correlation graph of gene expression changes (log_2 [fold-change]) between repeated ECS-treated and chronic SSRI-treated DGs. The gene probes (3,706) that showed significant changes by either ECS or SSRI treatment in microarray analysis are shown. Correlation coefficient (R) was calculated. (**B**) The number of gene probes that showed greater than 2-fold changes by either ECS- or SSRI-treatment are represented by Venn diagram. (**C**) Functional classification on the basis of the gene ontology (GO) terms. The gene probes showed greater than 2-fold changes by either ECS-treatment or SSRI-treatment, or both ECS- and SSRI-treatment were analyzed. P-value was calculated by a modified Fisher's exact test. Highly associated gene ontology terms ($P < 0.001$) were represented.

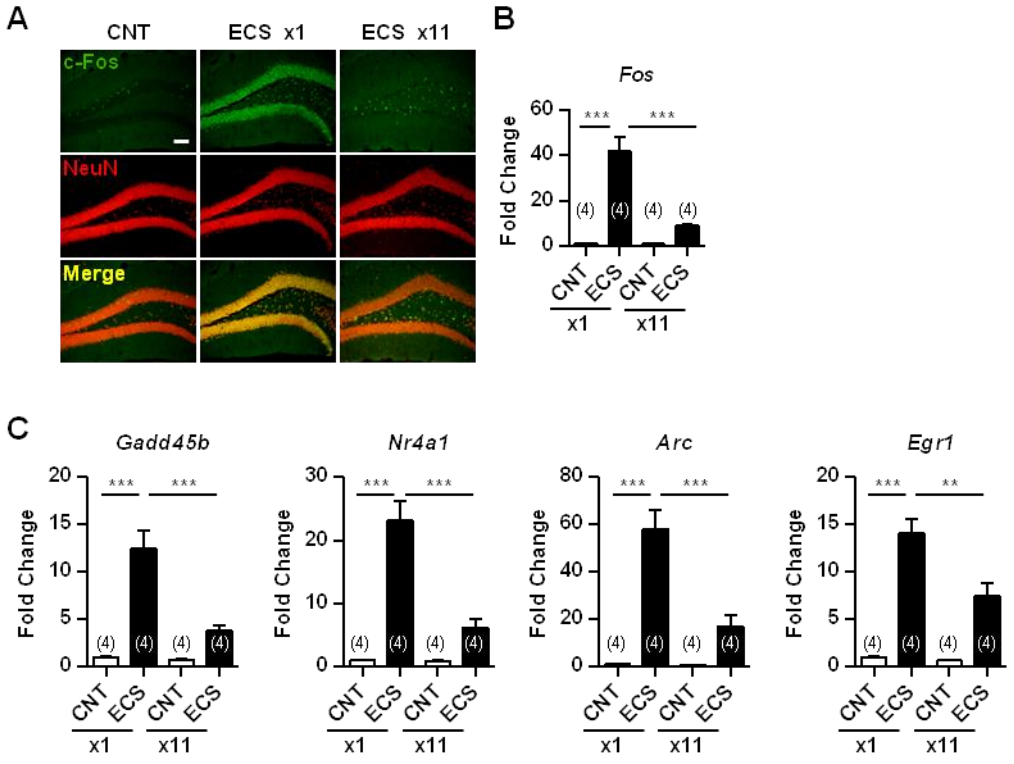

Figure 1-4. Attenuated stimulus-induced expression of IEGs in GCs after repeated ECS. (**A**) Representative images of immunoreactivity for c-fos and NeuN at 2 h after the last ECS. Scale bar, 100 μm. (**B**) The expression of *Fos* at 1 h after the last ECS (*** $P < 0.001$, Tukey's test following one-way ANOVA). (**C**) The relative expression of other IEG (*Gadd45b*, *Nr4a1*, *Arc*, and *Egr1*) mRNAs at 1 h after the last ECS (** $P < 0.01$, *** $P < 0.001$, Tukey's test following one-way ANOVA). The *n* numbers are given in parentheses. Data are presented as means ± SEM.

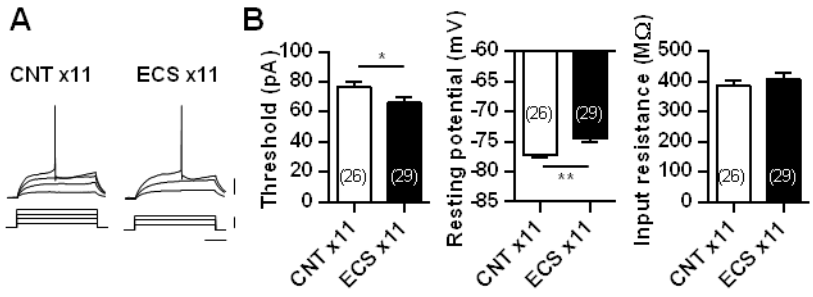

Figure 1-5. Immature-like functional properties of GCs after ECS. (**A**) Membrane potential changes (upper) induced by depolarizing currents (lower) in GCs. Scale bars: 100 ms, 20 mV, 40 pA. (**B**) Left: the threshold current intensity required to evoke a single spike (* $P < 0.05$). Middle: resting membrane potential (** $P < 0.005$). Right: input resistance. The *n* numbers represent the number of cells and are given in parentheses. Data are presented as means ± SEM.

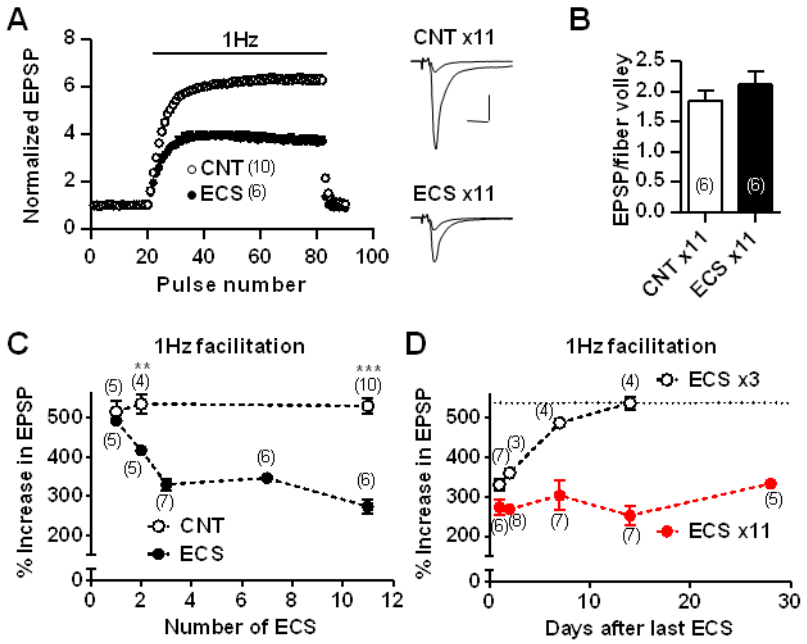

Figure 1-6. Reduction of 1Hz facilitation at the MF synapse after ECS. (**A**) Sample recordings of MF field EPSPs during baseline and 1 Hz stimulation after 11 times of ECS. Scale bars: 10 ms, 0.5 mV. (**B**) No significant effect of repeated ECS on the basal MF synaptic transmission. The relationship between basal field EPSP and fiber volley amplitude at the MF synapse was examined by changing stimulus intensities, and the slope value of regression line is shown as EPSP/fiber volley. (**C**) Reduction in frequency facilitation at the MF synapse after ECS repeated twice or more (** $P < 0.01$ *** $P < 0.001$). (**D**) Frequency facilitation tested at various time intervals after 3 times or 11 times of ECS. The *n* numbers are given in parentheses. Data are presented as means ± SEM.

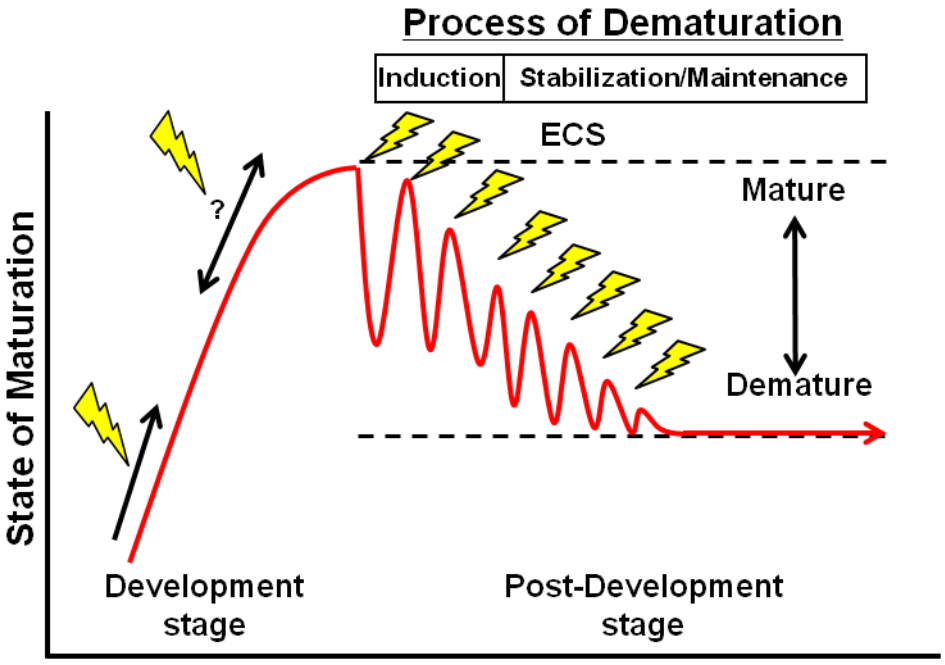

Figure 1-7. Model of activity-dependent regulation of state of granule cell maturation. Neuronal excitation facilitates the early phase of maturation and may also modulate the late maturation in developing cells. The process of ECS-induced dematuration in mature cells appears to involve separate phases; induction phase shortly after ECS, stabilization phase during repeated ECS period, and maintenance phase after repeated ECS procedures.

DISCUSSION

Neural activity is generally thought to promote differentiation and maturation process in neural development. Although it has been reported that the neural excitation facilitates the early phase of maturation steps in immature neurons (Ge et al., 2006; Overstreet-Wadiche et al., 2006; Zhao et al., 2012), the contribution of excitation to the late or terminal phase of maturation has been largely unknown. In this chapter, I showed that enhanced neural activation by ECS reverses the terminal maturation of hippocampal GCs and that repetitive neural activation converts the dematured state of GCs from a transient form to a long-lasting form, providing a novel regulatory mechanism of terminal maturation of GCs.

Neural activation reverses terminal GC maturation

After the treatments with ECS, GCs showed biochemical and physiological features resembling immature GCs. Although ECS can facilitate adult neurogenesis in the DG, the rapid reduction of mature GC markers after single ECS argues against the idea that such immature-like GCs are newly generated immature neurons. In addition, while newly generated immature neurons exhibit high input resistance mostly due to their small cell size, ECS-treated GCs showed normal input resistance. Thus, these results demonstrate that ECS reversed the biochemical and physiological phenotypes, but not the overall structural shape, of mature GCs into the immature-like state. The maturation stage marker analysis suggested that the state of the ECS-treated dematured GCs is comparable to that of late immature GCs.

The finding that enhanced excitation reverses the GC maturation is in striking contrast to previous results demonstrating that neuronal excitation, including excess activity caused by seizures, facilitates structural and functional maturation of GCs (Ge et al., 2006; Overstreet-Wadiche et al., 2006; Zhao et al., 2012). These opposite effects of excitation on neuronal maturation are most likely due to differences in the maturational stage of GCs. The facilitatory effects of excitation on GC maturation are typically observed in early postmitotic cells at the cell age around 2-3 weeks. For example, GABA-mediated depolarization in newborn GCs is essential for functional synapse formation and dendritic development within 2 weeks (Ge et al., 2006). The pilocarpine-induced seizures accelerated the dendritic extension and functional integration of newborn GCs at the cell age around 2 weeks (Overstreeet-Wadiche et al., 2006), and ECS-induced seizures during 4 weeks after the cell birth promoted morphological maturation of dendritic spines in newborn GCs (Zhao et al., 2012). On the other hand, in the present study, the reversing effect of ECS on GC maturation was

observed in fully matured GCs whose cell age should be more than 5 weeks based on the calbindin expression and stimulus-dependent expression of IEGs (Jessberger and Kempermann, 2003; Duan et al., 2008; Zhao et al., 2008). Therefore, the neural activity may differentially regulate GC maturation in a manner depending on the maturational state of neurons. It is possible that excitation consistently promotes both early and late maturation of GC development, and after GCs undergo terminal maturation, excitation can act to transform mature GCs to immature-like ones. The alternative possibility is that inhibitory signals can forward the late maturation of GCs, and neural activity may reverse the late maturation of GCs. Indeed, the intrinsic excitability of GCs decreases with their maturation (Schmidt-Hieber et al., 2004), and GABAergic synaptic inhibition increases at the late stage of GC maturation (Marin-Burgin et al., 2012).

Implication of GC dematuration in antidepressant actions and pathophysiological basis of other types of neuropsychiatric disorders

Previous reports have shown that SSRI treatment can induce GC dematuration (Koyabashi et al., 2010, 2011, and 2013). The phenotypes of the ECS-treated dematured GCs are indistinguishable from those of the SSRI-treated dematured GCs in many respects, as exemplified by similar comprehensive gene expression profiles in the DG. ECS has been considered to be an animal model of electroconvulsive therapy (ECT) for depression. In clinical use, ECT has fast-acting antidepressant effects and is effective in patients with resistance to monoaminergic antidepressant drugs. Consistent with this clinical setting, ECS rapidly induces GC dematuration, suggesting that neuronal dematuration in GCs is a common cellular basis underlying therapeutic effects of antidepressant treatments.

On the other hand, the immaturity of GCs is observed in several animal models associated with schizophrenia and related neuropsychiatric disorders (Ohira et al., 2013; Shin et al., 2013; Takao et al., 2013; Yamasaki et al., 2008), indicating that immature-like GCs do not simply exert therapeutic actions of neuropsychiatric disorders and may be involved in the pathogenesis of these diseases. Mice with immature or demature GCs show periodic hyperactivity in home cage activity (Kobayashi et al., 2011; Yamasaki et al., 2008), suggesting the implication of the immaturity of GCs in the behavioral destabilization. Since administration of excess SSRI is known to cause mania/psychosis behaviors in clinical settings, SSRI-induced dematuration may be implicated in these aversive effects of antidepressant treatments. However, given that depressive patients often show decreased energy expenditure and activity, it is possible that the periodic hyperactivity and/or other behaviors related to demature GCs may counteract some of depressive-like symptoms.

Chapter 2: Alteration of excitation/inhibition balance bidirectionally regulates maturation of granule cells in the dentate gyrus of the hippocampus

ABSTRACT

Neural activation by electroconvulsive stimulation (ECS) reverses the established mature state of granule cells (GCs) to the late immature stage in the dentate gyrus (DG). Brief neural activation by ECS initially triggers dematuration of GCs and repeated ECS stabilized the dematured phenotypes. However, the mechanisms underlying induction and stabilization of GC dematuration remain largely unknown. Here I show that activation of N-methyl-D-aspartate (NMDA) receptors is required for induction of the dematuration, and that alteration of excitation/inhibition balance affects the stabilization of dematured state of GCs. Treatment of mice with NMDA receptor antagonists significantly attenuated ECS-induced dematuration of GCs. The excitation/inhibition balance in GCs was shifted toward excitation after repeated ECS, and the augmentation of synaptic inhibition by diazepam prevented stabilization of the dematured state and promoted rematuration toward the matured state. These findings revealed that the terminal maturation of GCs is bidirectionally regulated; reversed and advanced by neuronal excitation and inhibition, respectively. The bidirectional regulation of the terminal maturation by neural activity suggests a unique approach to treat neuropsychiatric disorders by restoring the proper state of maturation via the control of neuronal excitability.

INTRODUCTION

In Chapter 1, I demonstrated that neural activation by electroconvulsive stimulation (ECS) rapidly induces dematuration of granule cells (GCs) in the adult dentate gyrus (DG), and repeated ECS stabilizes the dematured phenotypes of GCs. However, the mechanisms underlying induction and stabilization of dematuration in GCs remain unknown.

GC neurons receive the excitatory glutamatergic inputs from the entorhinal cortex through the perforant path (Figure 0-1) and inhibitory GABAergic inputs from local interneurons in the DG (Leranth and Hajszan, 2007). ECS is known to robustly activate excitatory glutamate signaling in the DG, and strongly upregulate expression of immediate early genes (IEGs) (Ma et al., 2009; Morinobu et al., 1997; Stewart and Reid, 1994), suggesting possible involvement of glutamate signaling in the regulation of GC dematuration by ECS. The functions of GCs are also regulated by monoaminergic and cholinergic signals, which directly act on GCs via their receptors or indirectly modify excitatory or inhibitory inputs (Leranth and Hajszan, 2007). Because it has been reported that the serotonin type 4 receptor (5-HT_4 receptor) is required for SSRI-induced dematuration of GCs (Kobayashi et al., 2010), serotonergic signaling may be also involved in the regulation of ECS-induced GC dematuration.

In this chapter, I explored the regulatory mechanisms underlying GC dematuration by ECS, by focusing on excitatory, inhibitory and serotonergic signals in the DG.

RESULTS

Involvement of NMDA receptor-dependent signaling in induction of GC dematuration

I firstly explored the signaling pathway involved in the induction of GC dematuration by ECS. Since ECS activates glutamate signaling in the hippocampus (Ma et al., 2009; Morinobu et al., 1997; Stewart and Reid, 1994), I examined whether N-methyl-D-aspartate receptor (NMDAR) is involved in the rapid induction of GC dematuration by using ketamine, an antagonist of NMDARs. A high dose (200 mg/kg) of ketamine inhibited the induction of expression of *Gadd45b* and *Fos*, but not that of *Egr1* (Figure 2-1), by single ECS, suggesting that ECS can activate both NMDAR-dependent and -independent signaling. This high dose of ketamine attenuated the reduction in *Calb1* and *Tdo2* expression by single ECS (Figure 2-2A). Ketamine also blocked the reduction in frequency facilitation at the mossy fiber (MF) synapse (Figure 2-2B). These effects are unlikely caused by lasting anesthetic action of ketamine, because an anesthetic dose of pentobarbital did not affect the reduction in expression of mature GC markers or frequency facilitation by ECS (Figures 2-2B and 2-2C). In addition, i.c.v. administration of D-AP5, another NMDAR antagonist, attenuated the downregulation of *Calb1* and *Tdo2* expression by ECS (Figure 2-2D). Thus, the rapid induction of dematuration by ECS requires NMDARs.

Since NMDAR activation up-regulates expression of many genes in DG, gene induction and subsequent *de novo* protein synthesis might be necessary for ECS-induced neuronal dematuration. As expected, pretreatment of mice with actinomycin D, a transcription inhibitor, or cycloheximide, a protein synthesis inhibitor, attenuated the reduction in the expression of mature GC markers by single ECS (Figures 2-3A and 2-3B). Actinomycin D alone substantially decreased the *Tdo2* mRNA level, but not that of *Calb1*, suggesting differential transcriptional regulation of these genes. The reduction in the synaptic facilitation was also attenuated by pretreatments with cycloheximide (Figure 2-3C). These results suggest that the protein synthesis following NMDAR activation is important for the rapid induction of neuronal dematuration by ECS.

I also examined whether the 5-HT_4 receptor is involved in the ECS-induced dematuration, because this receptor plays a key role in SSRI-induced GC dematuration (Kobayashi et al., 2010). However, neither deficiency of the 5-HT_4 receptor nor a lesion of the central serotonergic neurons with 5,7-dihydroxytryptamine (5,7-DHT) affected the reduction in the *Calb1* expression by ECS (Figures 2-4A-C). Therefore, the signaling pathway involved in the ECS-induced dematuration is distinct from that in the

SSRI-induced dematuration.

Role of GABAergic signaling in reversal of long-lasting dematuration

The above results showed that activation of excitatory synaptic transmission triggers the mature-to-demature state transition of GCs. I next explored the mechanism underlying the long-lasting dematuration. As described in Chapter 1, Dematured GCs show higher somatic excitability. To measure excitatory and inhibitory synaptic responses, whole-cell voltage-clamp recordings were conducted (Figure 2-5A). The amplitude of evoked inhibitory postsynaptic currents (IPSCs) relative to excitatory postsynaptic currents (EPSCs) was significantly reduced in ECS-treated GCs (Figure 2-5B). This raises a possibility that enhanced excitability caused by depressed inhibitory synaptic transmission is involved in the long-lasting dematuration. I therefore examined the role of GABAergic inhibition in regulating the maturation state of GCs. Diazepam, a positive allosteric modulator of $GABA_A$ receptor, was administered during and/or after the period of ECS treatments. Chronic diazepam treatment had no significant effect on frequency facilitation at the MF synapse in control mice (Figure 2-6A), suggesting a lack of effects on the matured state of GCs. In diazepam-treated mice, however, 11 times of ECS failed to induce a long-lasting reduction in frequency facilitation at 14 days after ECS (Figure 2-6B), and the reduction in the expression of mature GC markers, *Calb1* and *Tdo2*, was significantly reversed in 14 days after 11 times of ECS (Figure 2-6C, see Figures 1-1C and 1-1D for comparison). Thus, augmented GABAergic inhibition prevents stabilization of the dematured state.

The long-lasting dematuration appears to involve separate phases: induction, stabilization, and maintenance (Chapter 1). I therefore examined which phase of dematuration was affected by the augmented GABAergic inhibition. As described above, pentobarbital, an enhancer of $GABA_A$ receptor functions, did not block the rapid induction of dematuration by ECS (Figures 2-2B and 2-2C). Consistently, diazepam had no significant effect on the reduction in frequency facilitation at 1 day after 3 times of ECS (Figure 2-6D), suggesting that the enhanced GABAergic inhibition does not affect the induction of dematuration. However, diazepam applied during 11 times of ECS treatments slightly, but significantly, attenuated the reduction in frequency facilitation at 1 day after the last ECS, and the facilitation was completely restored to the control level in 14 days (Figure 2-6D), even when the diazepam treatment was discontinued after ECS. These results suggest that the enhanced GABAergic inhibition blocks stabilization of the dematuration state during repeated ECS. Finally, the effect of diazepam on the maintenance of dematuration was examined after repeated ECS. Diazepam applied only after 11 times of ECS treatments partially, but significantly, reversed the reduction in

frequency facilitation (Figure 2-6E), suggesting that the enhanced GABAergic inhibition promotes rematuration of GCs in the maintenance phase. Taken together, these results suggest that the enhanced GABAergic inhibition prevents the stabilization and maintenance phases, but not the induction phase, of dematuration, and that the terminal maturation of GCs is reversed and advanced by neuronal excitation and inhibition, respectively (Figure 2-7).

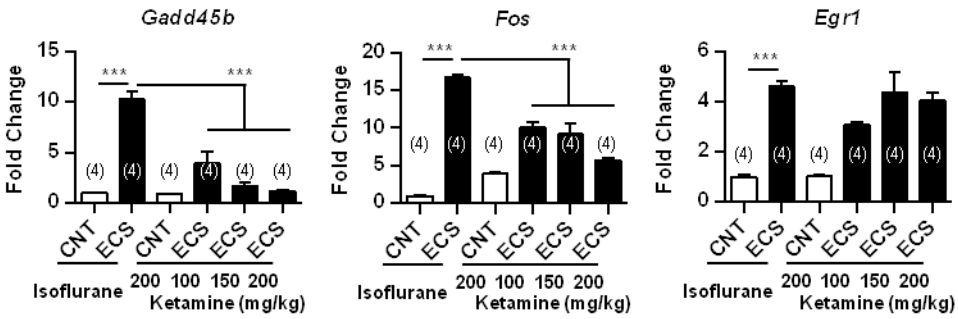

Figure 2-1. Effects of NMDAR antagonist on ECS-induced gene expression changes. Dose-dependent effects of ketamine on the induction of IEGs (*Gadd45b*, *Fos* and *Egr1*). Mice were intraperitoneally administered with ketamine at the indicated dose 15 min before ECS and expression of IEGs was analyzed at 2 h after single ECS (*** $P < 0.001$, Tukey's test following one-way ANOVA). The *n* numbers are given in parentheses. Data are presented as means ± SEM.

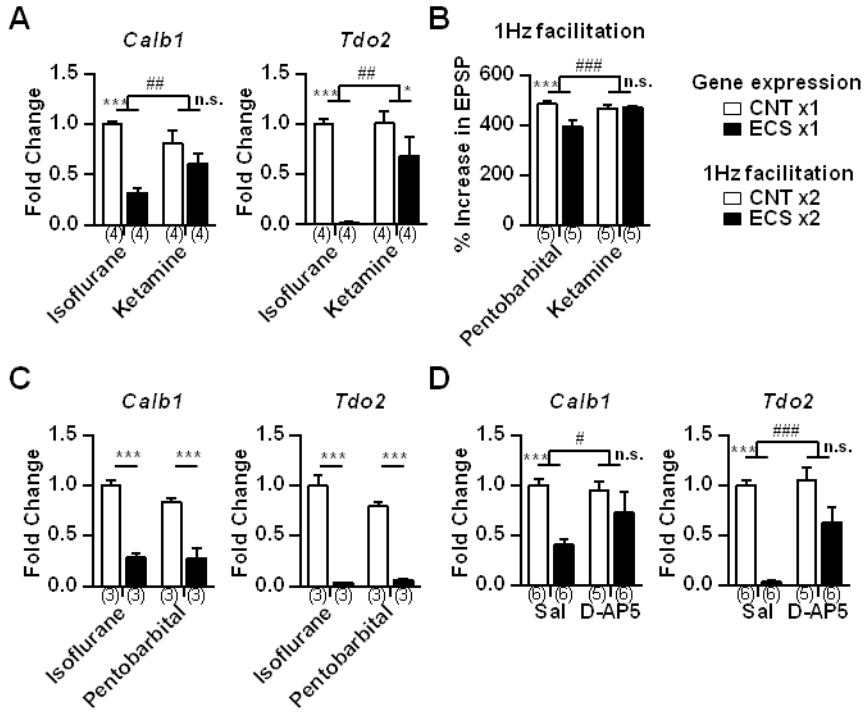

Figure 2-2. NMDA receptor activation is involved in rapid induction of neuronal dematuration by ECS. (**A, C, D**) The relative expression of *Calb1* and *Tdo2* at 6 h after single ECS in mice treated with drugs; (**A**) ketamine (200 mg/kg, i.p.), (**C**) pentobarbital (50 mg/kg, i.p.), or (**D**) D-AP5 (1 μg/mouse, i.c.v.). (**B**) Frequency facilitation at the MF synapse after two times of ECS. Mice were treated with ketamine (200 mg/kg, i.p.) 15 min before each ECS. The effect of ECS on *Calb*1 and *Tdo2* was attenuated by NMDA antagonists as indicated by significant interaction in 2-way ANOVA (drug treatment X ECS, # $P < 0.05$, ## $P < 0.01$, ### $P < 0.001$). The effect of ECS was tested by *Post-hoc* Bonferroni's test (* $P < 0.05$, ** $P < 0.01$, *** $P < 0.001$, n.s., not significant). The *n* numbers are given in parentheses. Data are presented as means ± SEM.

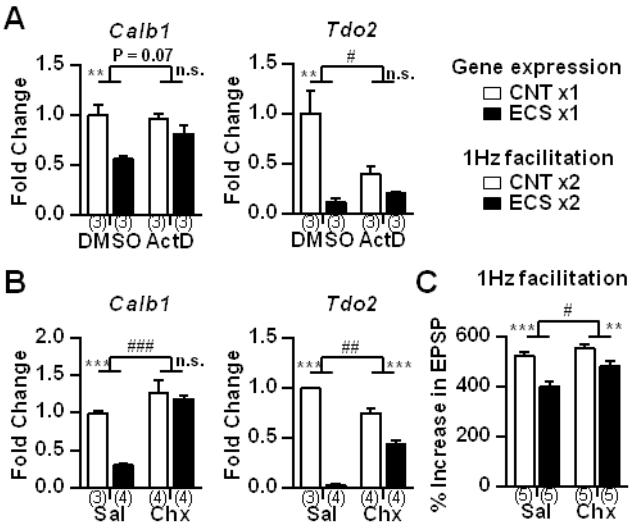

Figure 2-3. *de novo* synthesis of RNA and protein is involved in the rapid induction of neuronal dematuration by ECS. (**A, B**) The relative expression of *Calb1* and *Tdo2* at 6 h after single ECS in mice treated with drugs; (**A**) Actinomycin D (ActD; 50 μg/mice, i.c.v.), or (**B**) cycloheximide (Chx; 200 mg/kg, i.p. (**C**) Frequency facilitation at the MF synapse after two times of ECS. Mice were treated with cycloheximide (100 mg/kg, i.p.) 30 min before each ECS. The effect of ECS on *Calb*1 and *Tdo2* was attenuated by the drug treatment as indicated by significant interaction in 2-way ANOVA (drug treatment X ECS, # $P < 0.05$, ## $P < 0.01$, ### $P < 0.001$). The effect of ECS was tested by *Post-hoc* Bonferroni's test (* $P < 0.05$, ** $P < 0.01$, *** $P < 0.001$, n.s., not significant). The *n* numbers are given in parentheses. Data are presented as means ± SEM.

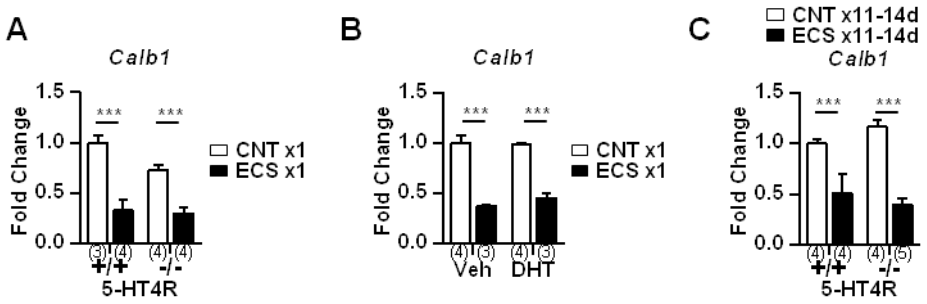

Figure 2-4. Serotonergic signals are NOT involved in the rapid induction of neuronal dematuration by ECS. (**A, B**) The relative expression of *Calb1* and *Tdo2* at 6 h after single ECS in (**A**) 5-HT4 receptor-deficient (-/-) mice or (**B**) mice treated with 5,7-dihydrotryptamine (DHT, i.c.v.). (**C**) The relative expression of *Calb1* was compared in 5-HT4 receptor-deficient (-/-) mice and wild-type (+/+) mice at 14 days after 11 times of ECS. * $P < 0.05$, ** $P < 0.01$, *** $P < 0.001$, n.s., not significant, Bonferroni's test following two-way ANOVA. The *n* numbers are given in parentheses. Data are presented as means ± SEM.

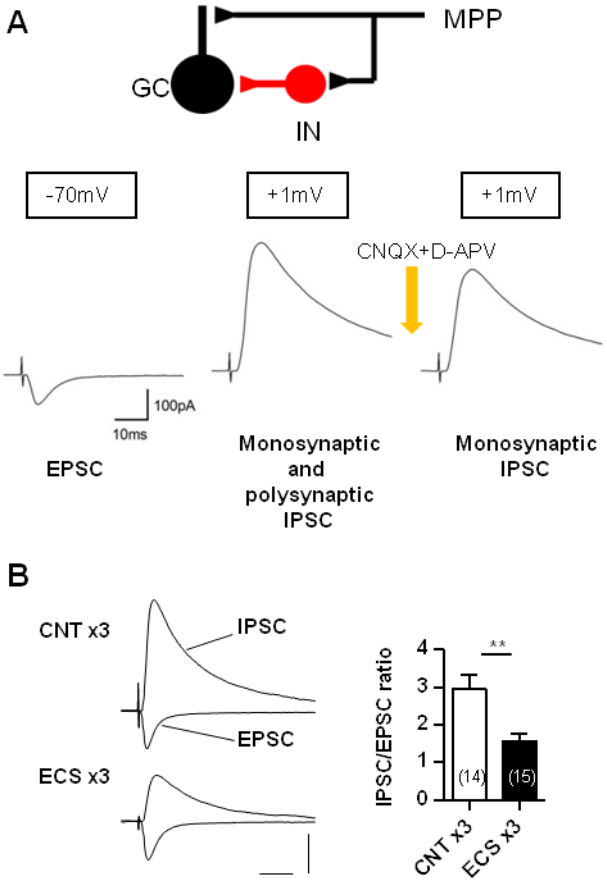

Figure 2-5. ECS reduces IPSC/EPSC ratio. (A) Top: schematic diagram of feedforward neuronal circuit. IN: inhibitory neuron. Bottom: sequential recordings of EPSC, IPSC including monosynaptic and polysynaptic components, and monosynaptic IPSC. Glutamate receptor antagonists were applied in order to prevent polysynaptic IPSC from the feedback circuit. Inhibitory neurons in the feedback circuit also contribute to IPSC in GCs. (**B**) Left, excitatory postsynaptic currents (EPSCs) and monosynaptic inhibitory postsynaptic currents (IPSCs) recorded in the same GCs. Right, reduced IPSC/EPSC ratios after 3 times of ECS (** $P < 0.01$, n represents number of cells). Scale bars: 20 ms, 100 pA. The *n* numbers are given in parentheses. Data are presented as means ± SEM.

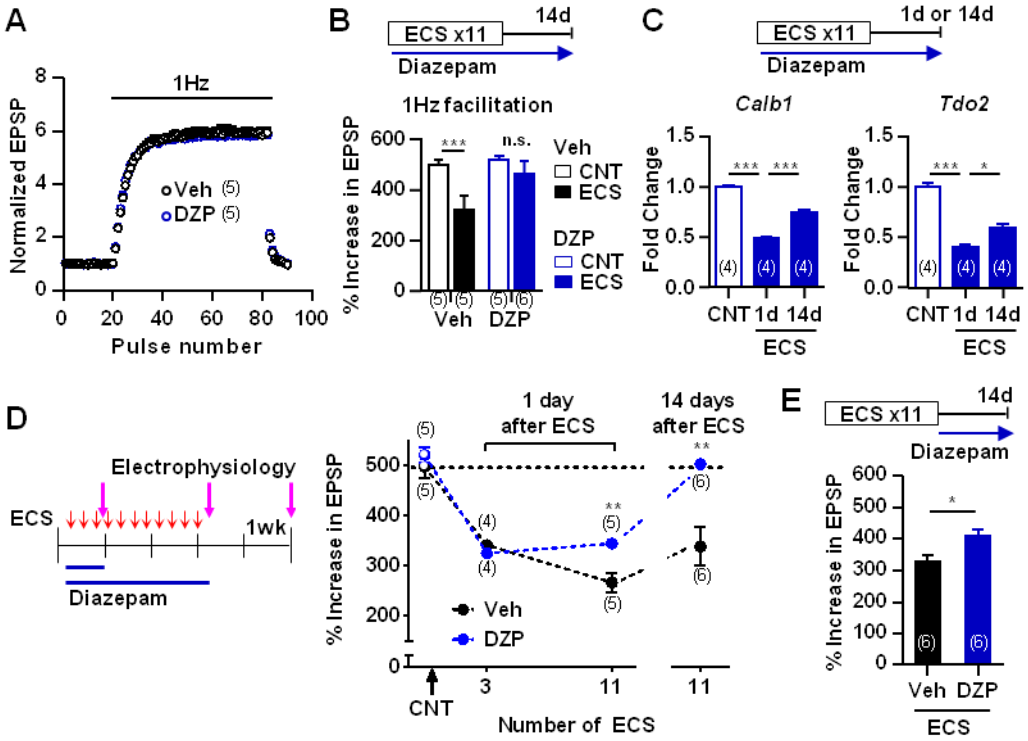

Figure 2-6. Augmentation of GABAergic signaling reverses long-lasting dematuration. (**A**) No significant difference in frequent facilitation at the MF synapse between mice treated with diazepam (DZP, 5 mg/kg) and vehicle (Veh) for 3 weeks. (**B**) Frequency facilitation at 14 days after 11 times of ECS in mice with 5 mg/kg diazepam or vehicle. The effect of ECS on frequency facilitation was attenuated by diazepam as indicated by significant interaction in 2-way ANOVA (drug treatment X ECS, P = 0.0146). The effect of ECS was tested by *Post-hoc* Bonferroni's test (*** P < 0.001, n.s., not significant). (**C**) The relative expression of *Calb1* and *Tdo2* at 1 day or 14 days after 11 times of ECS in mice treated with 10 mg/kg diazepam (* P < 0.05, *** P < 0.001, Tukey's test following one-way ANOVA). (**D**) Effects of 5 mg/kg diazepam on frequency facilitation at 1 day or 14 days after the indicated number of ECS. Diazepam was administered during the period of ECS treatments (** P < 0.01). (**E**) The effect of 10 mg/kg diazepam administered after 11 times of ECS on the lasting reduction of frequency facilitation (* P < 0.05). The *n* numbers are given in parentheses. Data are presented as means ± SEM.

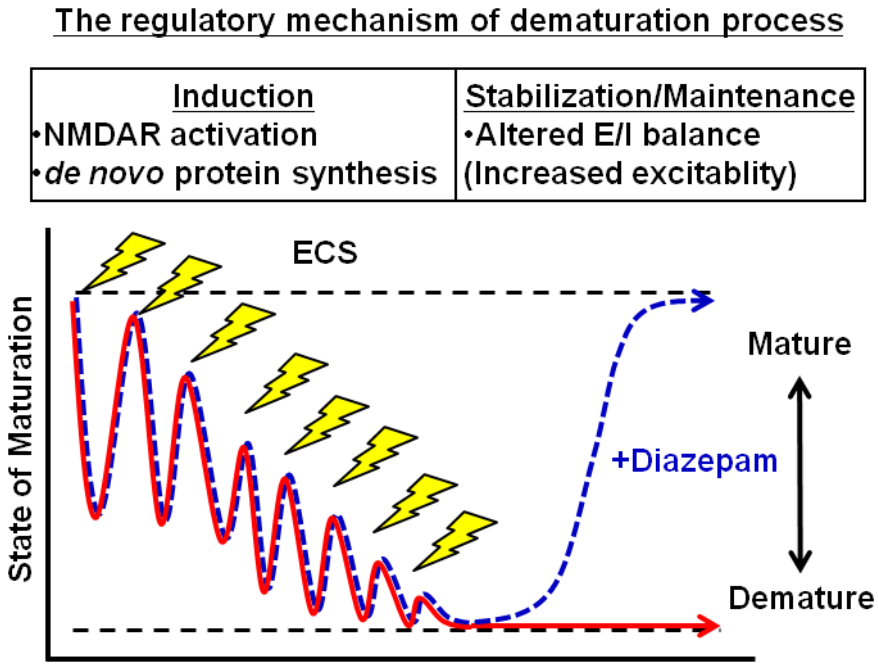

Figure 2-7. Schematic diagram showing activity-regulated transition between mature and demature states. Brief neural activation by ECS induces dematuration of GCs via NMDAR activation and *de novo* protein synthesis. Repetitive stimulation makes the demature state long-lasting. The dematured state is reversed by diazepam, showing increased excitability is based on stabilization or maintenance of the demature state.

DISCUSSION

In this chapter, I found that NMDARs play an essential role in induction of GC dematuration, and that GABAergic augmentation has an opposing effect. These results demonstrate that the terminal process of GC maturation can be reversed and advanced by neuronal excitation and inhibition, respectively, and the synaptic excitation/inhibition balance regulates the transition between the mature and dematured states (Figure 2-7).

Activity-dependent bidirectional regulation of terminal neural maturation

The rapid induction of dematuration by ECS is in contrast to the slowly developing SSRI-induced dematuration via Gs-coupled 5-HT_4 receptor signaling (Kobayashi et al., 2010). The induction of dematuration by ECS required NMDAR activation, induction of gene expression and subsequent *de novo* protein synthesis. An NMDAR-dependent increase in intracellular Ca^{2+} levels can activate multiple signaling pathways, such as calmodulin (CaM)-dependent adenylyl cyclases (type 1 and 8), CaM kinases, and Erk/MAP kinase cascades. Activation of these pathways promptly increases phosphorylation of several transcription factors, such as CREB (Davis et al., 2000). Indeed, CREB phosphorylation in GCs is consistently elevated immediately after a single ECS (Tanis et al., 2008). In contrast, it has been reported that SSRI increases hippocampal CREB phosphorylation after chronic, but not acute, treatment (Nibuya et al., 1996; Thome et al., 2000). In the developmental process of newborn GCs, CREB is highly phosphorylated until 3 weeks after birth (Nakagawa et al., 2002). Thus, CREB phosphorylation could be a common intracellular event required for ECS- and SSRI-induced dematuration. Therefore, prompt phosphorylation of CREB may play a critical role in the rapid induction of transcription-dependent dematuration by ECS.

Strong extrinsic stimulation, such as ECS, robustly induced dematured phenotypes in GCs, and after repeated stimulation, the dematured GCs exhibited higher somatic excitability (Chapter 1). In this chapter, I also demonstrated that synaptic excitation of dematured GCs is enhanced after ECS treatment, and that enhanced GABAergic inhibition promotes rematuration from the dematured state, suggesting that the enhanced excitability of dematured GCs autonomously stabilizes the dematured state, and enhanced inhibitory synaptic transmission of dematured GCs counteracts the stabilization process. As shown in this chapter, one of the key molecules that instruct the activity-dependent dematuration is NMDAR. Therefore, it is possible that the enhanced excitability of dematured GCs constantly activates NMDAR, which may support stabilization of the dematured state. Because NMDAR activation requires postsynaptic depolarization, enhanced GABAergic inhibition of dematured GCs would counteract the

NMDAR activation and attenuate the NMDAR-dependent signaling described above, thereby possibly permitting the terminal rematuration.

Regulation of neural maturation by E/I balance: implication in pathophysiology and treatment of different types of neuropsychiatric disorders

One of the common functional features of dematured GCs in SSRI- and ECS-treated mice is the increased somatic excitability. I found that ECS treatment changes the synaptic E/I balance toward excitation in GCs. It has been suggested that neural excitation or E/I balance in DG was perturbed by chronic stress. Repeated separation stress reduced the density of excitatory spine synapses in GCs (Poeggel et al., 2003), and chronic mild stress enhanced GABAA-mediated tonic inhibition in GCs (Holm et al., 2011) and reduced evoked neural activity in the DG (Airan et al., 2007). It is possible that GC dematuration restores the proper neural activity in the DG in the depressed state by enhancing synaptic and/or intrinsic excitability, although this possibility needs to be tested using depression or chronic stress models.

On the other hand, growing evidence has suggested that the altered E/I balance may be causally related to psychiatric disorders, such as autism spectrum disorders and schizophrenia (Coghlan et al., 2012; Kehrer et al., 2008). Recent studies have also suggested that immaturity of the DG is involved in a pathophysiological basis of schizophrenia and related neuropsychiatric disorders (Ohira et al., 2013; Shin et al., 2013; Takao et al., 2013; Walton et al., 2012; Yamasaki et al., 2008). Aberrant neural development could alter the circuit E/I balance, possibly due to insufficient maturation of the GABAergic network. Conversely, the altered E/I balance toward excitation may hamper the terminal neural maturation and stabilize the aberrant state of maturation in these disorders. Enhanced inhibition may have beneficial effects in this type of psychiatric disorders by correcting the circuit E/I balance and thereby allowing maturation of neurons in the circuit. Indeed, enhancing GABAergic inhibition has been suggested as a treatment protocol for schizophrenia (Gonzalez-Burgos et al., 2011). Restoring the normal matured state of neurons by proper modulation of neural activity could represent a possible fundamental remedy for these disorders.

Chapter 3: Involvement of mature granule cell dematuration in the adult neurogenesis in the dentate gyrus of the hippocampus

ABSTRACT

Chronic treatment with selective serotonin (5-HT) reuptake inhibitors (SSRIs) facilitates adult neurogenesis in the subgranular zone (SGZ) and dematuration in mature granule cells (GCs) in the dentate gyrus (DG) of the hippocampus. However, it is largely unknown whether dematuration of mature GCs is related to increased neurogenesis in the DG. Recent reports have suggested that 5-HT_4 receptor is involved in both the observed neurogenesis and GC dematuration. In this chapter, I addressed this issue using 5-HT_4 receptor knockout (5-HT4R KO) mice. Chronic treatment with the SSRI fluoxetine significantly increased cell proliferation and the number of doublecortin-positive cells in the DG of wild-type mice, but not in 5-HT4R KO mice. The neurogenic effect of fluoxetine was inversely correlated with the expression level of calbindin in the DG, indicating that increased neurogenesis is closely associated with progression of GC dematuration. Expression of neurogenic factors, such as brain-derived neurotrophic factor (BDNF), in the DG was also associated with the progression of GC dematuration. These results suggest that 5-HT_4 receptor-mediated phenotypic changes in mature GCs, including dematuration, may underlie the neurogenic effect of SSRIs in the DG, providing a new mechanism underlying adult neurogenesis in the hippocampus.

INTRODUCTION

The dentate gyrus (DG) of the hippocampus is one of the neurogenic regions in the adult brain, where new granule cells (GCs) are generated from neural stem cells. The generation of new GCs is influenced by various factors, including genetic background, environmental conditions, stress, and ageing (Zhao et al., 2008), and recent studies have implicated adult neurogenesis not only in learning and memory but also in pathology of neuropsychiatric disorders (Ming and Song, 2011). Chronic administration of antidepressants, such as selective serotonin (5-HT) reuptake inhibitors (SSRIs), increases adult neurogenesis in the DG (Malberg et al., 2000; Eisch et al, 2012), and a recent pharmacological study suggested that 5-HT_4 receptor partly mediates SSRI-induced neurogenic action in the DG (Mendez-David et al., 2014). Furthermore, it has been reported that 5-HT_4 receptor is essential for dematuration of GCs by chronic SSRI treatment (Kobayashi et al., 2010). However, it remains largely unknown how 5-HT_4 receptor contributes to both neurogenic and dematuration effects of chronic SSRI administration within the DG.

In this chapter, using 5-HT_4 receptor knockout (5-HT4R KO) mice with the C57BL/6J background, I explored regulatory roles of 5-HT_4 receptor in both neurogenesis and GC dematuration, and found that dematuration and accompanying changes in mature GCs mediated by the 5-HT_4 receptor underlies the neurogenic action of fluoxetine in the DG.

RESULTS

Involvement of the 5-HT_4 receptor in fluoxetine-induced neurogenic effects in the DG

Pharmacological studies using 5-HT_4 receptor agonists and antagonists have suggested that the 5-HT_4 receptor is involved in adult neurogenesis in the DG (Lucas et al., 2007; Mendez-David et al., 2014). However, there has been no study examining influence of genetic deficiency of the 5-HT_4 receptor on SSRI-induced neurogenesis in the DG. In this chapter, I examined effects of SSRI treatments on adult neurogenesis in 5-HT4R KO mice with the C57BL/6J background, and demonstrated involvement of the 5-HT_4 receptor in the fluoxetine-induced dematuration of GCs (Kobayashi et al., 2010).

Because it has been reported that the 5-HT content in the raphe nuclei is decreased in a distinct line of 5-HT4R KO mice with the 129/Sv background (Conductier et al., 2006), the contents of 5-HT and its main metabolite, 5-hydroxyindole acetic acid (5-HIAA), were measured in the hippocampus and the raphe nuclei in 5-HT4R KO mice with the C57BL/6J background. The total contents of 5-HT and 5-HIAA in both the hippocampus and the raphe nuclei were comparable in wild-type (WT) and 5-HT4R KO mice (Figure 3-1A) under basal conditions. An increase in extracellular 5-HT accumulation after a single administration of fluoxetine determined by *in vivo* microdialysis assay was not significantly different between the genotypes (Figure 3-1B). I also examined changes in the 5-HT and 5-HIAA contents by chronic fluoxetine treatment. Consistent with a previous report (Caccia et al., 1992), chronic fluoxetine reduced total contents of 5-HT and 5-HIAA in the hippocampus; the reduction in the 5-HT and 5-HIAA contents is likely to reflect feedback inhibition of 5-HT biosynthesis in the raphe nucleus. However, both the 5-HT and 5-HIAA contents after chronic fluoxetine treatment were not significantly different between WT and 5-HT4R KO mice (Figure 3-1C). These results show that the 5-HT turnover in the hippocampus is comparable in WT and 5-HT4R KO mice with the C57BL/6J background under both basal and fluoxetine-treated conditions. Thus, I used this mutant line to address whether the 5-HT_4 receptor is involved in SSRI-induced neurogenic activity in the DG.

Mice were intraperitoneally administered with 22 mg/kg/day fluoxetine for 21 days, and 5-Bromodeoxyuridine (BrdU) was given to label proliferating cells 2 h before sacrifice on the next day of the last fluoxetine administration (Figure 3-2A). The chronic fluoxetine treatment significantly increased the number of BrdU-positive cells in the subgranular zone (SGZ) of the DG compared with saline treatment in WT mice, whereas no significant difference was observed between saline and fluoxetine

treatments in 5-HT4R KO mice (Figures 3-2B and 3-2C). I next assessed the number of immature neurons by immunostaining for doublecortin (DCX), a marker of neurogenesis (Figures 3-2D and 3-2E). The number of DCX-positive cells in the DG was significantly increased in fluoxetine-treated WT mice, but not significantly changed in 5-HT4R KO mice. These results demonstrate that the neurogenic effect of chronic fluoxetine treatment in the DG is mediated by the 5-HT_4 receptor.

The 5-HT_4 receptor is expressed in mature GCs of the DG

It has been reported that the 5-HT_4 receptor is abundantly expressed in the DG (Tanaka et al., 2012; Warner-Schmidt et al., 2009). Consistent with this, I observed that 5-HT_4 receptor mRNA (*Htr4*) is mainly expressed in the GC layer, rather than in the SGZ, of the DG by *in situ* hybridization (Figure 3-3A). The expression level of *Htr4* in the DG was not significantly changed by chronic fluoxetine treatment (control, 1.000 ± 0.091; fluoxetine, 1.348 ± 0.152, $p = 0.079$, $n = 6$ each). To determine the cell types expressing the 5-HT_4 receptor in the DG, I examined β-galactosidase immunoreactivity (LacZ-IR) in the hippocampus of the 5-HT4R KO mice, in which the β-galactosidase gene is 'knocked-in' at the *Htr4* gene locus. I found that the LacZ-IR was co-localized with the immunoreactivity of a neural marker, NeuN, and that of a marker for mature GCs, calbindin. However, LacZ-IR was not co-localized with the immunoreactivity of DCX, a marker for neural progenitors and immature neurons, or that of calretinin, a marker for immature GCs, in the SGZ (Figure 3-3B), indicating that the 5-HT_4 receptor is mainly expressed in mature GCs.

The neurogenic effect of fluoxetine is correlated with dematuration of GCs in the DG

The 5-HT_4 receptor is necessary for fluoxetine-induced GC dematuration (Kobayashi et al., 2010). Dematured GCs exhibit various phenotypic changes, including reduced expression of mature GC markers, increased somatic excitability, and reduced activity-dependent synaptic facilitation (Figure 0-2, and also see Chapters 1 and 2). Because expression of the 5-HT_4 receptor in the DG is mainly restricted to mature GCs, I hypothesized that progression of GC dematuration via the 5-HT_4 receptor is correlated with the neurogenic effect of fluoxetine within the SGZ of the DG. To address this hypothesis, I examined the expression level of the mature GC marker, calbindin, since the calbindin level was used as an index of GC dematuration (Kobayashi et al., 2010). Chronic fluoxetine treatment significantly reduced calbindin-IR in both the GC layer and molecular layer of the DG in WT mice, but not in 5-HT4R KO mice (Figures 3-4A and 3-4B). To examine the correlation between the neurogenic effect and the

dematuration effect of fluoxetine, I compared the number of proliferating cells and calbindin-IR in the DG of the same animals, and found that the number of proliferating cells was inversely correlated with calbindin-IR (Figure 3-4C). It is known that antidepressant treatment increases expression of neurotrophic factors and neuropeptides, including *Bdnf* and neuropeptide Y (*Npy*), in the DG (Nibuya et al., 1995; Sillaber et al., 2008), which has been implicated in enhanced neurogenesis (Decressac et al., 2011; Li et al., 2008; Scharfman et al., 2005). I therefore examined the correlation between the increased expression of these factors and the reduced expression of calbindin mRNA (*Calb1*) by RT-qPCR in the individual fluoxetine-treated DG in comparison with the average expression levels in the control DG. I found that the changes in the expression of *Bdnf* and *Npy* were inversely correlated with that of *Calb1* (Figure 3-4D). These results demonstrate that the neurogenic effect of fluoxetine in the SGZ is closely associated with the progression of GC dematuration in the DG.

Dematuration of GCs by chronic fluoxetine treatment occurs without adult neurogenesis

I finally examined whether the increased neurogenesis affects the dematuration of GCs by fluoxetine. To address this point, I used X-ray irradiation to block generation of new neurons within the SGZ, and examined the effect of fluoxetine on the reduction in calbindin-IR in the neurogenesis-depleted DG. Whole brain area was irradiated with X-rays 2 weeks before initiation of the fluoxetine treatment (Figure 3-5A). I confirmed that X-ray irradiation dramatically depleted the DCX-positive cells in the DG of both saline- and fluoxetine-treated mice (Figure 3-5B). The calbindin-IR in the DG did not change by the X-ray irradiation. However, chronic fluoxetine treatment significantly reduced the calbindin-IR even in the X-ray-irradiated mice (Figures 3-5C and 3-5D), although the extent of the reduction in calbindin expression was less dramatic in the X-ray-irradiated mice compared with sham-treated mice (Figures 3-5C and 3-5D). These results suggest that the increased neurogenesis is not critical for GC dematuration by fluoxetine treatment.

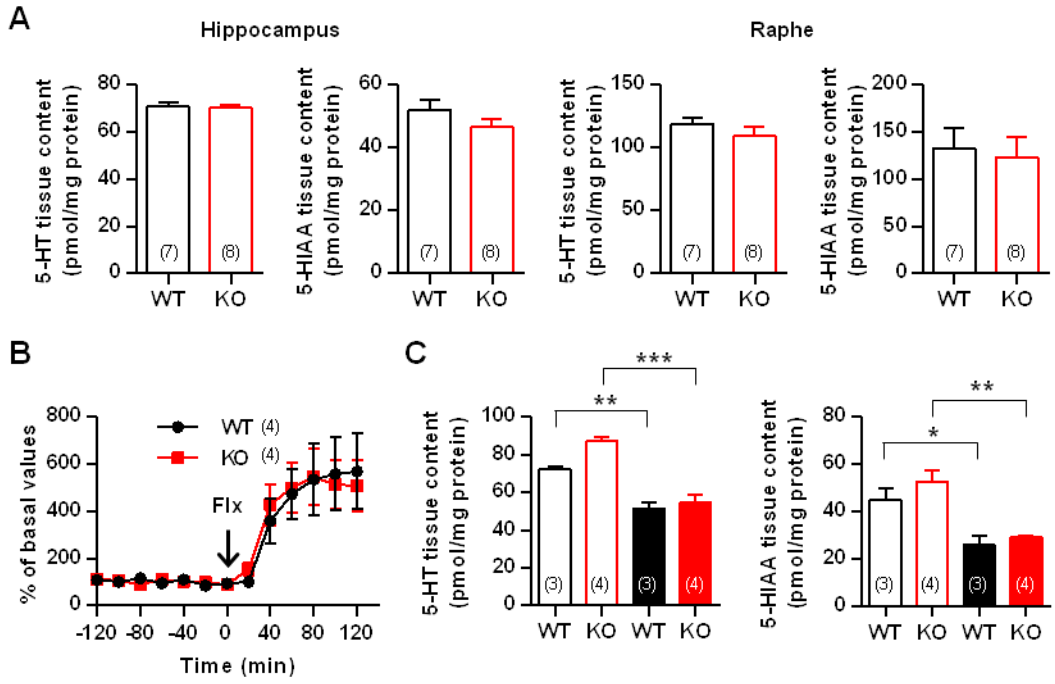

Figure 3-1. 5-HT levels in the hippocampus of 5-HT4R KO mice with the C57BL/6J-background. (**A**) Tissue 5-HT and 5-HIAA levels in the hippocampus and raphe nuclei. Data are expressed as means ± SEM. The *n* numbers are given in parentheses. (**B**) Fluoxetine (Flx)-induced increase in extracellular 5-HT concentrations in the hippocampus. After equilibration, dialysate samples were collected every 20 min with fluoxetine (22 mg/kg) administered at time zero. The average value of seven basal samples for each animal was defined as 100% and used for normalization. Data are expressed as means ± SEM. The *n* numbers are given in parentheses. (**C**) Tissue 5-HT and 5-HIAA levels in the hippocampus after chronic fluoxetine treatment. Fluoxetine (22 mg/kg/day) was administered for 3 weeks. Data are expressed as means ± SEM, with *, **, *** indicating significant differences ($P < 0.05$, $P < 0.01$, $P < 0.001$). The *n* numbers are given in parentheses.

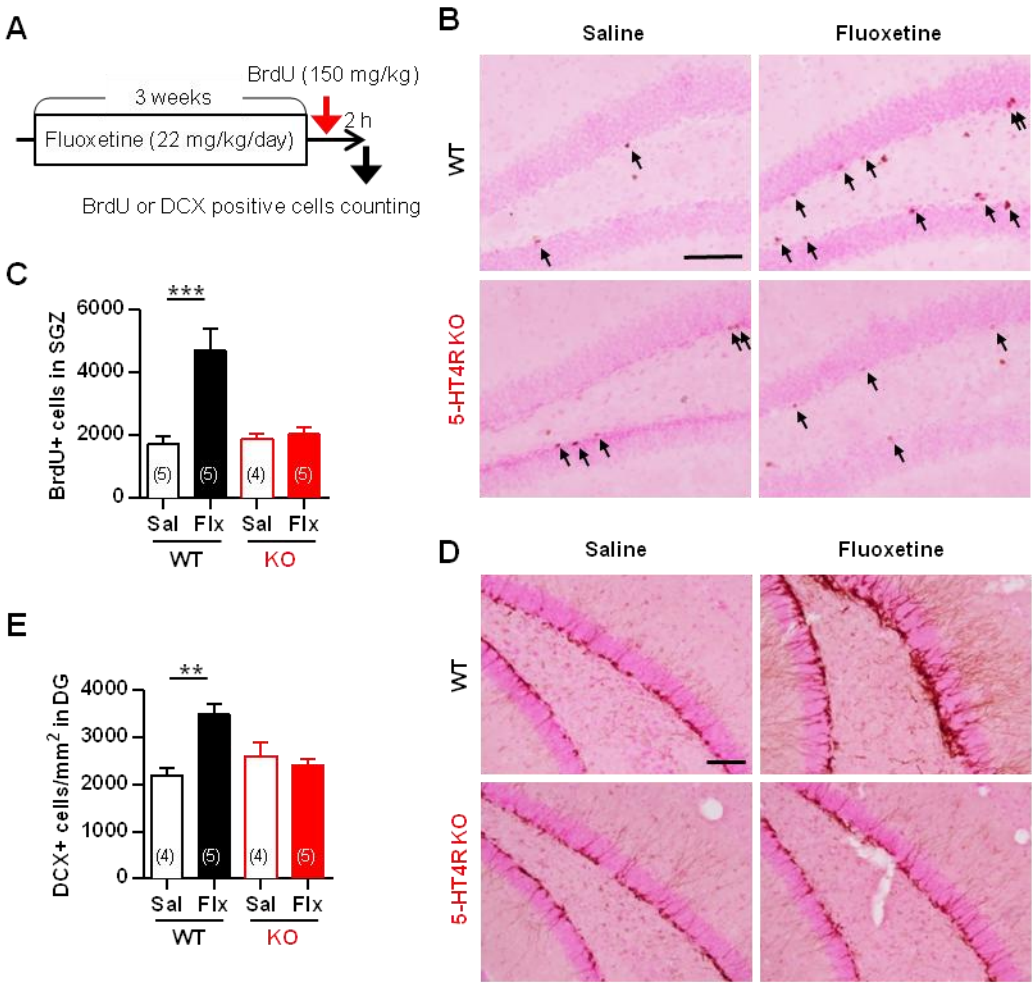

Figure 3-2. Effect of chronic fluoxetine treatment on adult neurogenesis in 5-HT4R KO mice. (**A**) Experimental scheme. Mice were IP-injected with fluoxetine (Flx) at a dose of 22 mg/kg/day for 3 weeks and were administered with BrdU 24 h after the last treatment at a dose of 150 mg/kg. Mice were sacrificed 2 h after the BrdU injection. (**B**) Immunohistochemical visualization of BrdU in the SGZ of the DG. Scale bar: 100 µm. Arrows indicate BrdU-positive cells. (**C**) Quantification of BrdU-positive cells in the SGZ of the DG in WT and 5-HT4R KO mice. Data are expressed as means ± SEM, with *** indicating significant differences ($P < 0.001$). The *n* numbers are given in parentheses. (**D**) Representative images of anti-doublecortin (DCX) immunohistochemistry in the DG. Scale bar: 100 µm. (**E**) Quantification of DCX-positive immature neurons in the DG of the WT and 5-HT4R KO mice. The number of DCX-positive cells in the DG is shown as the number of cells per square millimeter of the DG area. Data are expressed as means ± SEM, with ** indicating significant differences ($P < 0.01$). The *n* numbers are given in parentheses.

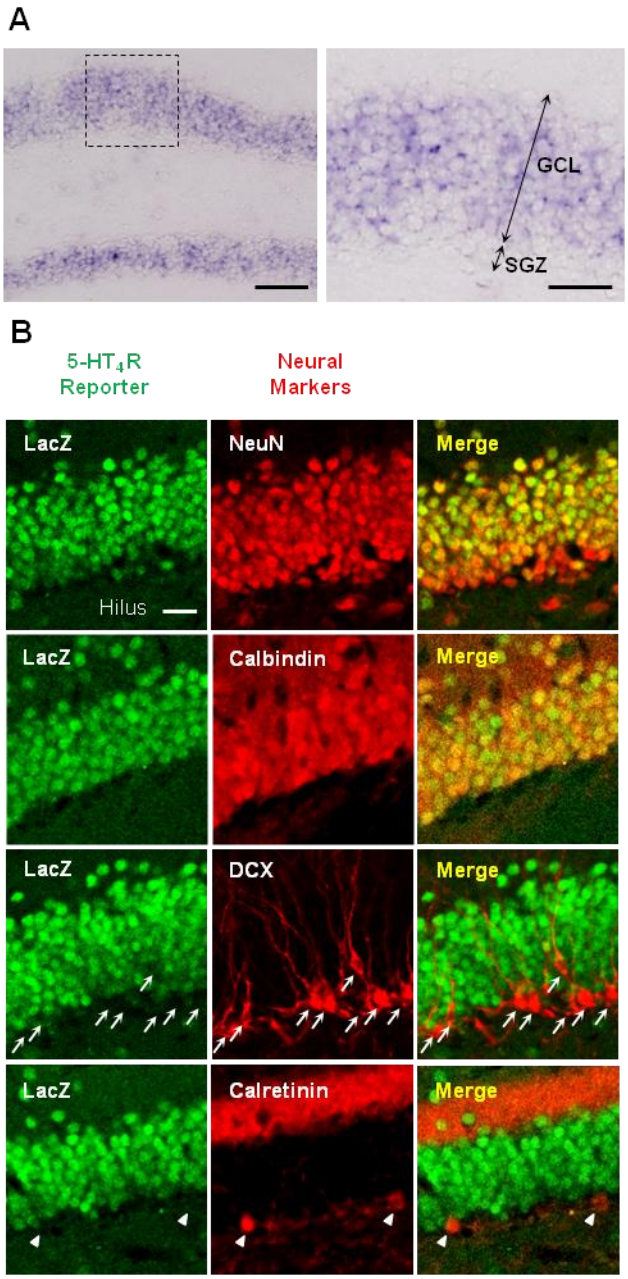

Figure 3-3. Expression of the 5-HT$_4$ receptor in the DG. (**A**) *in situ* hybridization analysis of 5-HT$_4$ receptor mRNA. GCL: granular cell layer, SGZ: subgranular zone. Scale bars: 100 μm (left) and 30 μm (right). (**B**) Representative images of immunostaining for β-galactosidase (LacZ) and markers of granule cells; NeuN, calbindin, doublecortin (DCX), and calretinin. Scale bar: 20 μm. Arrows and arrowheads indicate DCX- and calretinin-positive cells, respectively.

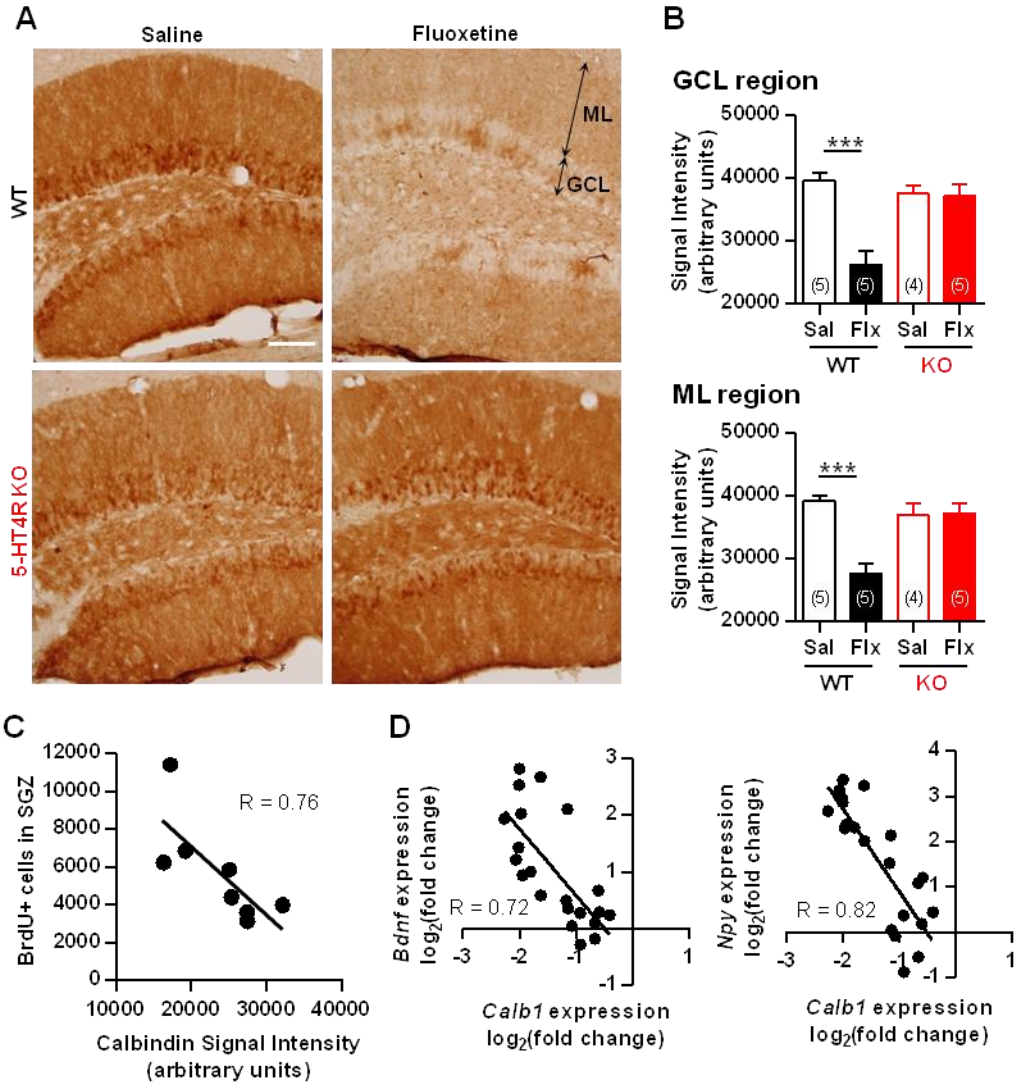

Figure 3-4. Correlation between enhancement of adult neurogenesis and GC dematuration. (**A**) Representative images of calbindin-IR. GCL: granule cell layer, ML: molecular layer. Scale bar: 100 µm. (**B**) Quantification of calbindin-IR in the GCL and the ML in WT and 5-HT4R KO mice. Data are expressed as means ± SEM, with *** indicating significant differences ($p < 0.001$). The *n* numbers are given in parentheses. (**C**) Comparison of the numbers of BrdU-positive cells in the SGZ and calbindin-IR of GCL region in WT mice. Mice received fluoxetine (22 mg/kg/day) for 3 or 4 weeks were plotted in the analysis. The correlation coefficient (R) was calculated ($P = 0.0278$). (**D**) Comparison of gene expression changes after chronic fluoxetine treatment between calbindin (*Calb1*) and *Bdnf* or *Npy*. Gene expression was normalized by the average gene expression in control mice. Mice received fluoxetine (22 mg/kg/day) for 3 or 4 weeks. Four independent experiments were included in this analysis. The correlation coefficient (R) was calculated (*Bdnf* vs. *Calb1*, $P = 0.0002$, *Npy* vs. *Calb1*, $P < 0.0001$).

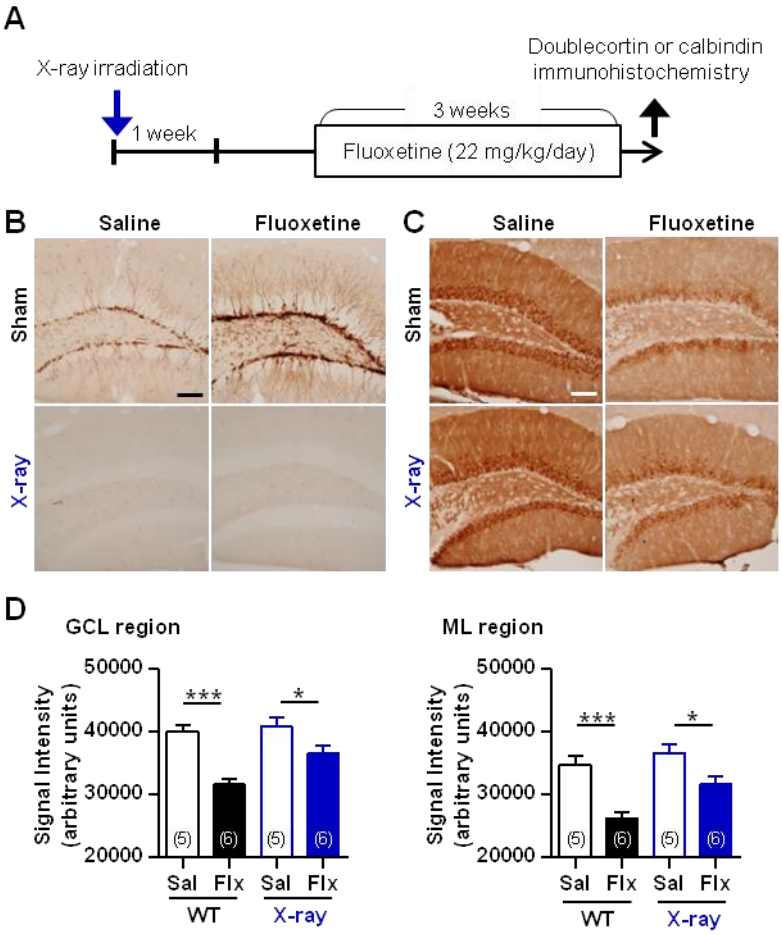

Figure 3-5. Effect of X-ray irradiation on fluoxetine-induced adult neurogenesis and dematuration in the DG. (**A**) Experimental scheme. Mice were irradiated with X-rays (10 Gy) 2 weeks before initiation of fluoxetine treatment. (**B** and **C**) Representative images of DCX (**B**) and calbindin (**C**) immunohistochemistry. Scale bars: 100 µm. (**D**) Quantification of calbindin-IR signal intensity in the GCL and ML in control (Sham) and X-ray-irradiated mice. Data are expressed as means ± SEM. Significance interaction between X-ray irradiation and Flx was calculated using 2-way ANOVA (GCL region, $P = 0.1089$, ML region, $P = 0.2085$). The effect of Flx was tested by *Post-hoc* Bonferroni's test (* $P < 0.05$, *** $P < 0.001$). The *n* numbers are given in parentheses.

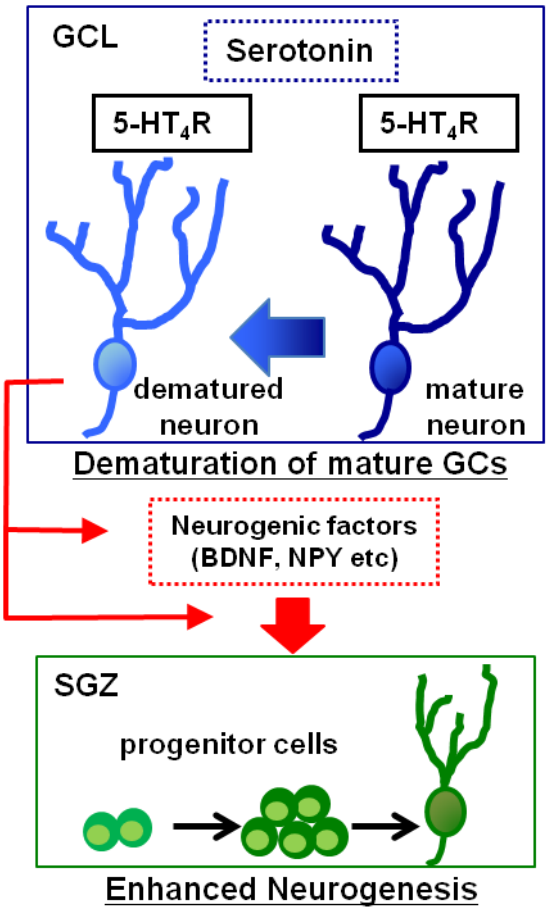

Figure 3-6. Model of 5-HT$_4$ receptor-mediated increase in neurogenesis in the DG induced by SSRIs. Increased serotonin accumulation after SSRI treatment stimulates postsynaptic 5-HT$_4$ receptors (5-HT$_4$R) on mature GCs and consequently induces GC dematuration. Dematured GCs produce increased levels of neurogenic factors, which may be involved in enhanced adult neurogenesis in the SGZ. GCL: granule cell layer, SGZ: subgranular zone.

DISCUSSION

In this chapter, I demonstrated that the 5-HT_4 receptor plays an important role in both enhanced adult neurogenesis in the DG and dematuration of GCs after chronic SSRI treatment, and that the increased neurogenesis is closely associated with the progression of GC dematuration. I further found that the 5-HT_4 receptor is mainly expressed in mature GCs and not in their progenitor cells in the SGZ. Altogether, these results suggest that 5-HT_4 receptor-mediated dematuration and accompanying changes in mature GCs underlie the neurogenic effects of SSRI treatment in the DG (Figure 3-6).

Relationship between increased neurogenesis and dematuration of GCs in the DG

I showed that the neurogenic effect of fluoxetine is closely associated with the progression of GC dematuration in the same animals. This association is supported by the facts that fluoxetine-induced neurogenesis and GC dematuration showed a similar dose and time dependency in C57BL/6 background mice (Kobayashi et al., 2010; Navailles et al., 2008; Wu and Castren, 2009) and both effects of fluoxetine were augmented by chronic corticosterone administration, a model of the anxiety and depressive-like state (David et al., 2009; Kobayashi et al., 2013). In addition, heterozygous α-calcium/calmodulin-dependent protein kinase II (α-CaMKII) mutant mice, Shunurri-2 KO mice, and pilocarpine-treated mice also exhibited enhanced adult neurogenesis concurrently with immaturity of GCs (Takao et al., 2013; Shin et al., 2013; Yamasaki et al., 2008), showing the correlation of two adjacent cellular changes in other cases.

However, the reduction in calbindin expression by SSRI was observed without newly generated neurons in the DG under X-ray irradiation, suggesting that dematuration of GCs occurred without increased neurogenesis. Considering the localization of the 5-HT_4 receptor and its requirement for both GC dematuration and increased neurogenesis by fluoxetine treatment, these results raise a possibility that dematuration-related phenotypic changes in mature GCs are involved in increased adult neurogenesis in the DG. However, I could not exclude a possibility that external factors affected by serotonergic neurons may simultaneously promote dematuration and neurogenesis, respectively.

How can dematuration and accompanying changes of GCs enhance adult neurogenesis in the DG? One possibility is that expression of neurogenic factors is increased in the DG with dematured GCs. I showed that expression of *Bdnf* and *Npy* in the DG is increased by chronic fluoxetine treatment, and that the increased expression is correlated with progression of GC dematuration. Central administration of NPY and

BDNF was reported to promote hippocampal neurogenesis (Decressac et al., 2011; Scharfman et al., 2005). It has also been reported that ablation or blockade of the BDNF receptor, TrkB, prevents fluoxetine-mediated stimulation of mitosis of progenitor cells (Li et al., 2008; Pinnock et al., 2010), suggesting implication of BDNF signaling in neurogenic effects of fluoxetine. Thus, the increased expression of these neurogenic factors in the DG with dematured GCs is likely to mediate enhanced adult neurogenesis. The dematured state of GCs may persistently activate signaling pathways to increase expression of these neurogenic factors.

Another possibility is that microcircuits are altered in the hippocampus. The DG with dematured GCs shows alteration in the E/I balance toward more excitable conditions (Chapter 2), and dematured GCs exhibit enhancement of monoamine-induced synaptic potentiation at the mossy fiber synapse (Kobayashi et al., 2010; 2012). Given that parvalbumin-positive GABAergic interneurons in the DG receive excitatory inputs from GCs (Seress et al., 2001), dematured GCs could affect functions of these GABAergic interneurons. It has been reported that GABAergic signals from parvalbumin interneurons directly stimulate neural progenitors and modulate adult neurogenesis in the SGZ (Song et al., 2012; 2013). Therefore, dematured GCs may modulate adult neurogenesis via GABAergic signals in the DG.

Behavioral effects of GC dematuration in the DG induced by SSRI treatment

Dematuration of mature GCs is assumed to have an impact on hippocampus-related and neurogenesis-independent behaviors, because the majority of neural population in the DG is composed of mature GCs (Ninkovic et al., 2007). Recent reports showed that antidepressant-like behaviors induced by chronic fluoxetine treatment were mediated by X-ray-sensitive and -insensitive processes (David et al., 2009; Mendez-David et al., 2014). Because I showed that X-ray irradiation blocked adult neurogenesis, but spared dematuration of GCs after chronic fluoxetine treatment, it is likely that the behaviors blocked by X-ray irradiation are closely associated with neurogenesis and that GC dematuration may contribute to X-ray-insensitive, antidepressant-like behaviors. Chronic fluoxetine treatment induced behavioral destabilization of home cage behaviors and this behavioral instability was attenuated in the 5-HT4R KO mice (Kobayashi et al., 2011). Because 5-HT_4 receptor deficiency abolished both neurogenic and dematuration effects of fluoxetine in the DG, it is difficult to interpret which cellular changes contribute to the behavioral changes in the 5-HT4R KO mice. In the future study, comparison of the behavioral effects of fluoxetine between WT and 5-HT4R KO mice under blockade of adult neurogenesis by X-ray will help to understand GC dematuration-associated behaviors.

CONCLUSION

The summary of the results presented in this study as follows:

Chapter 1

1. Neural activation by electroconvulsive stimulation (ECS) transiently reverses mature phenotypes of granule cells (GCs) in the dentate gyrus (DG) to immature-like phenotypes.
2. Repeated ECS stabilizes immature-like phenotypes of GCs.

These results suggest that neural activation reverses terminal maturation of GCs to a immature-like state; the reversal process is called as dematuration.

Chapter 2

1. Glutamatergic signals via the NMDA receptor is critical for ECS-induced dematuration of GCs in the DG.
2. Augmentation of synaptic inhibition by diazepam induces rematuration of dematured GCs.

These results suggest that the altered excitatory/inhibitory balance bidirectionally regulates terminal maturation of GCs.

Chapter 3

1. Chronic treatment with selective serotonin reuptake inhibitor (SSRI) induces enhanced adult neurogenesis in the DG and dematuration of GCs via the 5-HT_4 receptor.
2. The 5-HT_4 receptor is expressed in mature GCs, but not in neural progenitor cells or immature GCs.
3. Enhanced adult neurogenesis and progression of dematuration are significantly correlated with each other during chronic SSRI treatment.

These results suggest a new hypothesis that dematured GCs enhance adult neurogenesis in the DG during chronic SSRI treatment.

The present study demonstrated a novel regulatory mechanism of terminal maturation of GCs via the altered E/I balance in the DG and suggested a unique interaction between newborn neurons and pre-existing neurons. This study will provide a new insight into the physiological basis underlying neuropsychiatric disorders, and contribute to a possible fundamental remedy for these disorders.

MATERIALS AND METHODS

Chapter 1

Animals

Male C57BL/6J or C57BL/6N mice, 8 weeks of age, were purchased from Japan SLC or Charles River Japan. Mice were pair-housed and maintained under standard conditions with a 12-h light/dark cycle and *ad libitum* access to food and water unless otherwise stated. The 5-HT4 receptor mutant mice (strain name: B6.129P2-Htr4<tm1Dgen>/J) backcrossed to the C57BL/6J background were purchased from the Jackson Laboratory. Male and female homozygous mutant mice and their wild-type littermates from heterozygous mating were used in this study. All mice were habituated for over one week before experimental procedures. Animal use and procedures were in accordance with the National Institute of Health guidelines and approved by the Committee of Animal Research of Kyoto University, Faculty of Pharmaceutical Sciences and the Animal Care and Use Committee of Nippon Medical School.

Electroconvulsive stimulation

Bilateral ECS (current, 25 mA; shock duration, 1 sec; frequency, 100 pulse/sec; pulse width, 0.5 msec) was administered via moistened, spring-loaded ear-clip electrodes with a pulse generator (ECT Unit; Ugo Basile) to mice that were anesthetized with isoflurane (1.5 to 2%) in most experiments or pentobarbital (50 to 60 mg/kg) in order to avoid sudden unexpected death associated with seizures. In repeated treatments, ECS was administered 4 times a week for up to 3 weeks. The sham-treated animals were handled in an identical manner to the ECS-treated animals without the administration of shock.

Fluoxetine treatment

Fluoxetine hydrochloride (LKT Labs) was dissolved in drinking water and orally applied at a dose of 22 mg/kg/day for 4 weeks as described previously (Kobayashi et al., 2010). The fluoxetine solutions were prepared every day, and daily fluoxetine intake was determined for individual mice on the basis of the water consumption during the preceding 24 h and the body weight measured every other day. Saccharin (0.2%) was included in the fluoxetine solution to keep water intake comparable to the baseline.

Microarray analysis

For microarray analysis, samples were collected as follows. Mice were decapitated after the 11 times of ECS or 4 weeks treatment of fluoxetine at a dose of 22 mg/kg. The hippocampal slices were prepared as described below. The DG was dissected from some of them, and the remaining slices were used for electrophysiological analyses. Frequency facilitation at the mossy fiber-CA3 synapse was measured in each mouse, and the DG samples from fluoxetine-treated mice, which exhibited small frequency facilitation, were used as dematured DG (n = 3). Reduced facilitation was also confirmed in ECS-treated mice (see text). The control DG samples were collected from vehicle- or sham-treated mice. Total RNA was extracted from the samples using an RNeasy micro kit (Qiagen) and the RNAs of the same groups were put together. From each group, 100 ng of total RNA was amplified using a 3'IVT Express kit (Affymetrix, Inc.). All amplified RNAs were hybridized to the GeneChip mouse genome 430A 2.0 array (Affymetrix, Inc.), and the microarray suite 5.0 of the Affymetrix gene chip operating software was used for the analysis of the GeneChip data. For each transcript represented on the array, the statistical expression algorithm computes detection (present or absent), signal intensity, change (increase or decrease), and change p-value. If the average signal intensity was lower than 50 in all of the conditions (ECS, Sham, FLX, CNT), the genes were excluded from further analysis. Gene ontology analysis was performed using DAVID Bioinformatics Resources 6.7 (National Institute of Allergy and Infectious Diseases). All data were deposited at the GEO server (GSE54307).

Electrophysiological analysis

Mice were singly housed under the institutional standard conditions (14:10 light/dark cycle; lights on at 6:00 A.M. through 8:00 P.M.). Mice were decapitated under deep halothane anesthesia 24 h after the last ECS unless otherwise stated. Both hippocampi were isolated, and transverse hippocampal slices (380 μm) were cut using a tissue slicer. Electrophysiological recordings were performed as described (Kobayashi et al., 2010). Recordings were made in a submersion-type chamber maintained at 27.0 - 27.5 ºC and superfused at 2 ml/min with saline composed of (in mM): NaCl, 125; KCl, 2.5; NaH_2PO_4, 1.0; $NaHCO_3$, 26.2; glucose, 11; $CaCl_2$, 2.5; $MgCl_2$, 1.3 (equilibrated with 95% O_2 / 5% CO_2). Field excitatory postsynaptic potentials (fEPSPs) arising from the mossy fiber synapses were evoked by stimulating the dentate GC layer and recorded from the stratum lucidum of CA3 using a glass pipette filled with 2 M NaCl. The amplitude of fEPSPs was measured on analysis as described (Kobayashi et al., 2007). A criterion used to identify the mossy fiber input was more than 85% block of fEPSP by an agonist of group II metabotropic glutamate receptors,

(2S,2'R,3'R)-2-(2',3'-dicarboxycyclopropyl)glycine (DCG-IV, 1 μM). Single electrical stimulation was delivered at a frequency of 0.05 Hz unless otherwise specified. The initial slope of fEPSPs was measured on analysis. The fiber volley amplitude was measured in the presence of 6-cyano-7-nitroquinoxaline-2,3-dione (CNQX, 10 μM) and D-(-)-2-amino-5-phosphonopentanoic acid (D-AP5, 25 μM). Whole-cell current-clamp recordings were made from the granule cells with a pipette filled with a solution composed of (in mM) potassium gluconate 140, HEPES 20, NaCl 8, MgATP 2, Na_2GTP 0.3, EGTA 0.05 (pH adjusted to 7.3 with KOH). The recording pipette was placed in the middle third of the granule cell layer. Hyperpolarizing currents (6 - 16 pA, 400 ms) were injected through the recording pipette to measure the input resistance. Depolarizing currents (400 ms) with increasing intensity by 10 pA steps were injected to measure the threshold current intensity to evoke action potentials. The liquid junction potential was corrected in these recordings. All recordings were made using a Multiclamp 700B amplifier (Molecular Devices, Sunnyvale, CA, USA), filtered at 2 kHz and stored in a personal computer via an interface (digitized at 5 - 10 kHz). DCG-IV was purchased from Tocris Bioscience (Bristol, UK).

Immunohistochemistry

Mice were perfused with saline and 4% paraformaldehyde (PFA) in 0.1 M phosphate buffer, pH 7.4. The brains were dissected out and postfixed in the same fixative at 4˚C for 24 h. After immersion in 0.1 M phosphate buffer containing 20% sucrose at 4˚C overnight, the brains were rapidly frozen at -80˚C and sectioned using a cryostat at 30 μm thickness. The free-floating sections were first incubated with 10% normal equine serum in PBS containing 0.3% Triton X-100 for 1 h at room temperature and subsequently incubated with mouse anti-calbindin-D-28K monoclonal antibody (Sigma Aldrich, C9848, diluted 1:3000), mouse anti-calretinin monoclonal antibody (Millipore, MAB 1568, diluted 1:3000), goat anti-doublecortin polyclonal antibody (Santa Cruz, sc-8066, diluted 1:500), rabbit anti-c-Fos polyclonal antibody (Calbiochem, PC38, diluted 1:2000), or mouse anti-NeuN antibody (Millipore, MAB377, diluted 1:500) overnight at 4˚C. After washing three times with PBS containing 0.3% Triton X-100, the sections were incubated with secondary antibody conjugated with AlexaFluor488 or AlexaFluor555 (Molecular Probes). After washing, the sections were mounted on slide glasses and observed with a fluorescent microscope (Biozero 8000, Keyence).

Immunoblotting

The brains were removed at 24 h after the last ECS and the DG of the hippocampus was dissected under a stereoscopic microscope. The isolated DG was sonicated in protein

lysis buffer containing a protease inhibitor cocktail (Nacalai Tesque) on ice and centrifuged at 20,000 *g* at 4˚C for 10 min. Supernatants containing 10 μg of proteins were separated on 12% SDS-polyacrylamide gel by electrophoresis and transferred onto a PVDF membrane. The membrane was first blocked with Blocking One (Nacalai Tesque) at room temperature for 1 h and then incubated with mouse anti-calbindin-D-28K monoclonal antibody (diluted 1:3000) at 4˚C overnight. After washing, the membrane was incubated with horseradish peroxidase-conjugated secondary antibody (Jackson ImmunoResearch Laboratories) at room temperature for 1 h, and bands were visualized with ECL reagents (GE Healthcare). The same membrane was then stripped, and detected with mouse anti-β-actin monoclonal antibody (Millipore, MAB1501R, diluted 1:3000) in the same way. The signal intensity of calbindin was calculated by LAS-3000 (FujiFilm) and normalized to that of β-actin.

Real time PCR

Mice were decapitated at the indicated time in figure legends. Total RNA was extracted from the isolated DG by using an RNeasy micro kit (Qiagen) or Reliaprep RNA Cell Miniprep System (Promega), and subjected to the reverse transcription reaction with a Superscript VILO (Invitrogen), followed by real time PCR with a LightCycler (Roche Applied Science) using Fast Start DNA Master SYBR Green I. Crossing point values were acquired by using the second derivative maximum method. The expression level of each gene was quantified using external standardized dilutions. Relative expression levels of target genes between samples were normalized to that of 18S rRNA. Primer sequences for each gene are shown in Table 1. The specificity of each primer set was confirmed by checking the product size by gel electrophoresis.

***In situ* hybridization**

In situ hybridization was performed using a digoxigenin (DIG)-labeled probe. *Calb1* cDNA for probe template was cloned by PCR with gene-specific primers (forward; 5'-actgaccacagcggcttc-3', reverse; 5'-agaggcagaagcccatcc-3', Product Length; 927 bp), verified by sequencing, and used to produce a labeled riboprobe with an RNA Labeling kit (Roche). The brains were removed from mouse skulls at 6 h after single ECS and rapidly frozen on dry ice. Coronal brain sections (thickness 10 μm) were cut on a cryostat, mounted onto slide glasses, fixed in 4% paraformaldehyde, acetylated, and dehydrated prior to hybridization. Sections were hybridized with the DIG-labeled riboprobe and visualized using an alkaline phosphatase (AP)-conjugated anti-DIG antibody and a BM purple substrate (Roche). None of the sense probes yielded any specific signal (data not shown).

Statistics

All data are presented as means ± SEM. Experiments with two groups were compared with unpaired two-tailed Student's *t* test unless otherwise specified, and experiments with more than two groups were subjected to one-way ANOVA, followed by the Dunnett's test or the Tukey's test. Interaction between subgroups was compared with two-way ANOVA, followed by the Bonferroni's test. Statistical significance was set at $P < 0.05$. The number of data "*n*" represents the number of mice used unless otherwise specified.

Chapter 2

Animals

Male C57BL/6J or C57BL/6N mice, 8 weeks of age, were purchased from Japan SLC or Charles River Japan. Mice were pair-housed and maintained under standard conditions with a 12-h light/dark cycle and *ad libitum* access to food and water unless otherwise stated. All mice were habituated for over one week before experimental procedures. Animal use and procedures were in accordance with the National Institute of Health guidelines and approved by the Committee of Animal Research of Kyoto University, Faculty of Pharmaceutical Sciences and the Animal Care and Use Committee of Nippon Medical School.

Electroconvulsive stimulation

Bilateral ECS (current, 25 mA; shock duration, 1 sec; frequency, 100 pulse/sec; pulse width, 0.5 msec) was administered via moistened, spring-loaded ear-clip electrodes with a pulse generator (ECT Unit; Ugo Basile) to mice that were anesthetized with isoflurane (1.5 to 2%) in most experiments or pentobarbital (50 to 60 mg/kg) in order to avoid sudden unexpected death associated with seizures. In repeated treatments, ECS was administered 4 times a week for up to 3 weeks. The sham-treated animals were handled in an identical manner to the ECS-treated animals without the administration of shock.

Drug treatments

Diazepam (Wako) was dissolved in DMSO at 10 to 20 mg/ml, diluted in the drinking water, and administered at 5 to 10 mg/kg/day. D-AP5 (Tocris Bioscience) was dissolved in saline and intracerebroventricularly administered (1 μg/mouse) under anesthesia with pentobarbital (50 mg/kg) 20 min prior to ECS. Actinomycin D (Santa Cruz) was dissolved in DMSO and intracerebroventricularly administered (50 μg/mouse) under

anesthesia with pentobarbital (50 mg/kg) 20 min prior to ECS. Ketamine (Daiichi Sankyo Propharma) was intraperitoneally administered at a dose of 200 mg/kg, and ECS was delivered 15 min later without further anesthesia. Cycloheximide (Santa Cruz) was dissolved in saline and intraperitoneally administered at a dose of 100 mg/kg (for electrophysiological analysis) or 200 mg/kg (for gene expression analysis) 30 min before or after ECS. For deletion of serotonergic neurons, 5,7-dihydroxytryptamine (5,7-DHT; Sigma Aldrich) was dissolved in saline containing 0.1% ascorbic acid and was intracerebroventricularly administered (200 μg/mouse) under anesthesia with pentobarbital (50 mg/kg) 30 min after intraperitoneal injection of desipramine (25 mg/kg; Sigma Aldrich). The deletion of serotonergic neurons 1 week after the injection was confirmed in equally conditioned mice by immunohistochemical analysis using anti 5-HT antibody (Immunostar 20080, diluted 1:10000) (data not shown). For electrophysiological experiments, injection of ketamine or cycloheximide was repeated after a 48 h interval, and hippocampal slices were prepared 24 h after the second ECS. CPP (Sigma-Aldrich) was dissolved in saline and intraperitoneally injected at a dose of 20 mg/kg shortly after ECS procedures.

Electrophysiological analysis

Mice were singly housed under institutional standard conditions (14:10 light/dark cycle; lights on at 6:00 A.M. through 8:00 P.M.). Mice were decapitated under deep halothane anesthesia 24 h after the last ECS unless otherwise stated. Both hippocampi were isolated, and transverse hippocampal slices (380 μm) were cut using a tissue slicer. Electrophysiological recordings were performed as described (Kobayashi et al., 2010). Recordings were made in a submersion-type chamber maintained at 27.0 - 27.5 ºC and superfused at 2 ml/min with saline composed of (in mM): NaCl, 125; KCl, 2.5; NaH_2PO_4, 1.0; $NaHCO_3$, 26.2; glucose, 11; $CaCl_2$, 2.5; $MgCl_2$, 1.3 (equilibrated with 95% O_2 / 5% CO_2). Field excitatory postsynaptic potentials (fEPSPs) arising from the mossy fiber synapses were evoked by stimulating the dentate GC layer and recorded from the stratum lucidum of CA3 using a glass pipette filled with 2 M NaCl. The amplitude of fEPSPs was measured on analysis as described (Kobayashi et al., 2007). A criterion used to identify the mossy fiber input was more than 85% block of fEPSP by an agonist of group II metabotropic glutamate receptors, (2S,2'R,3'R)-2-(2',3'-dicarboxycyclopropyl)glycine (DCG-IV, 1 μM). Single electrical stimulation was delivered at a frequency of 0.05 Hz unless otherwise specified. The initial slope of fEPSPs was measured on analysis. Whole-cell voltage-clamp recordings were made from the granule cells with a pipette filled with a solution composed of (in mM) cesium gluconate 140, HEPES 20, NaCl 8, EGTA 0.1, MgATP 2, Na_2GTP 0.3 (pH

adjusted to 7.3 with CsOH). Excitatory postsynaptic currents (EPSCs) evoked by MPP stimulation were recorded at the reversal potential (-70 mV) for inhibitory postsynaptic currents (IPSCs). The amplitude of EPSC was adjusted around 100 pA. Monosynaptic IPSCs were then recorded in the same cells at +1 mV in the presence of CNQX (10 μM) and D-APV (25 μM) (see Figure 2-5A). The liquid junction potential was corrected in these recordings. All recordings were made using a Multiclamp 700B amplifier (Molecular Devices, Sunnyvale, CA, USA), filtered at 2 kHz and stored in a personal computer via an interface (digitized at 5 - 10 kHz). DCG-IV, CNQX and D-AP5 were purchased from Tocris Bioscience (Bristol, UK).

Real time PCR

Mice were decapitated at the indicated time in figure legends. Total RNA was extracted from the isolated DG by using an RNeasy micro kit (Qiagen) or Reliaprep RNA Cell Miniprep System (Promega), and subjected to the reverse transcription reaction with a Superscript VILO (Invitrogen), followed by real time PCR with a LightCycler (Roche Applied Science) using Fast Start DNA Master SYBR Green I. Crossing point values were acquired by using the second derivative maximum method. The expression level of each gene was quantified using external standardized dilutions. Relative expression levels of target genes between samples were normalized to that of 18S rRNA. Primer sequences for each gene are shown in Table 1. The specificity of each primer set was confirmed by checking the product size by gel electrophoresis.

Statistics

All data are presented as means ± SEM. Experiments with two groups were compared with unpaired two-tailed Student's *t* test unless otherwise specified, and experiments with more than two groups were subjected to one-way ANOVA, followed by the Dunnett's test or the Tukey's test. Interaction between subgroups was compared with two-way ANOVA, followed by the Bonferroni's test. Statistical significance was set at $P < 0.05$. The number of data "*n*" represents the number of mice used unless otherwise specified.

Chapter 3

Animals

All mice were housed under standard illumination parameters with a 12-h light/dark

cycle and *ad libitum* access to water and food. Male 5-HT_4 receptor heterozygous mutant mice that had been backcrossed to the C57BL/6J background for 10 generations were purchased from the Jackson Laboratory (Bar Harbor, ME, USA). Male (6-12 weeks old) wild-type (WT) and homozygous mutant (5HT4R KO) mice prepared by heterozygous mating were used as previously described (Kobayashi et al., 2010; 2011). For cranial irradiation experiment, C57BL/6N mice (5 weeks old) were purchased from Japan SLC (Hamamatsu, Japan) and habituated for over one week before experimental procedures. All experimental procedures were approved by the Committee of Animal Research of Kyoto University Faculty of Pharmaceutical Sciences.

Cranial irradiation

Mice (6 weeks of age) were anesthetized with pentobarbital (50 mg/kg; Kyoritsu Pharma), and exposed to cranial irradiation using a Rigaku Radiofrex 350 X-ray generator operated at 250 kV and 15 mA with a 1-mm-thick aluminum filter. X-rays at a dose of 10 Gy were delivered at a dose rate of 0.74 Gy/min. A lead shield was placed over the body of the mice except the head. Non-irradiated controls received anesthesia only. Fluoxetine treatment was started 2 weeks after irradiation.

SSRI treatment

Fluoxetine hydrochloride (LKT laboratories, Inc., St. Paul, MN, USA) was intraperitoneally injected at a dose of 22 mg/kg for 21 days. The fluoxetine solution was prepared every day. Control mice were intraperitoneally injected with saline. For experiments comparing gene expression in the DG, some mice were given fluoxetine hydrochloride dissolved in 0.2% of saccharin solution and orally applied at a dose of 22 mg/kg for 28 days. Concentration of fluoxetine were determined for individual mice based on the consumption during preceding 24 h and the body weight measured every other day (Kobayashi et al., 2010). Control mice were orally given water.

Measurement of tissue monoamine contents and *in vivo* microdialysis

Tissue 5-HT and 5-HIAA contents were measured as previously described with some modifications (Nagayasu et al., 2010). Briefly, 1-mm-thick coronal slices were prepared using a brain matrix on ice. Then, tissue blocks containing the dorsal raphe nucleus and median raphe nucleus or hippocampus were dissected, homogenized, and sonicated in 300 μL of ice-cold 0.1 M $HClO_4$ containing 10 mM $Na_2S_2O_5$ and 1 mM EDTA. Protein concentrations were determined using a Bradford protein assay (Bio-Rad, Hercules, CA, USA). Homogenates were centrifuged at 16,000 × *g* at 4°C for 15 min, and supernatants

were stored at -80°C until use. Supernatants were thawed on ice and analyzed by high-performance liquid chromatography with an electrochemical detector (HPLC-ECD) (Eicom, Kyoto, Japan). The measured 5-HT concentration was normalized against the total protein concentration. The detection limits for both 5-HT and 5-HIAA were estimated to be approximately 0.5–0.6 fmol per 25 μL of sample.

For *in vivo* microdialysis, mice were stereotactically implanted with a guide cannula (Eicom) in the ventral hippocampus according to the atlas of Franklin and Paxinos (2008) with the following coordinates: anterior-posterior, -2.8 mm from the bregma; lateral, 3.0 mm from the mid line; dorsal-ventral, -2.5 mm from the skull surface. Experiments were performed 1 day after surgery in awake and freely moving mice. On the day of the experiment, a dialysis probe with a length of 1 mm (Eicom) was inserted into the guide cannula and perfused with Ringer's solution (147 mM NaCl, 4 mM KCl, 3 mM $CaCl_2$) at a flow rate of 1 μL/min for 2–3 h. After the initial perfusion period, dialysate samples were collected every 20 min. On-line quantification of 5-HT in the dialysate was accomplished by HPLC-ECD, and seven basal samples were collected before fluoxetine administration. Fluoxetine (22 mg/kg) was then administered intraperitoneally and samples were collected for an additional 120 min. The average values of the seven basal samples for each animal were defined as 100% and used for normalization. Probe placement in each mouse was histologically verified by examining the coronal brain sections after completion of the experiment.

Immunohistochemistry

On the next day of the last treatment, mice received BrdU (150 mg/kg, IP., Sigma B5002). Two hours after BrdU injection, the mice were anesthetized by chloral hydrate (Nacalai Tesque, Kyoto, Japan) and transcardially perfused with cold saline followed by 4% PFA in 0.1 M phosphate buffer, pH 7.4. Brains were postfixed with 4% PFA at 4°C overnight, cryoprotected in 20% sucrose overnight, and stored at -80°C. Serial sections were then cut through the entire hippocampus (Segi-Nishida et al., 2008) at 30-μm-thick with a cryostat (Leica CM3050) and stored in a non-freezing solution at -20°C until stained.

For BrdU immunostaining, every sixth section was mounted on glass slides and incubated in 0.01 M citric acid at 90°C for 5 min, denatured with 2 M hydrogen chloride at 37°C for 30 min, neutralized with 0.1 M boric acid (pH 8.5) at room temperature for 10 min, blocked in 10% equine serum in PBS containing 0.3% Triton X-100 at room temperature for 60 min, and incubated with monoclonal rat anti-BrdU (1:200; Serotec OBT0030) at room temperature overnight. For DCX and calbindin immunostaining, sections were blocked in 10% equine serum and incubated with

polyclonal goat anti-DCX (1:500; Santa Cruz SC8066) or monoclonal mouse anti-calbindin D-28K (1:3000; Sigma Aldrich, C9848). Sections were then incubated for 60 min with biotinylated goat anti-rat IgG (1:1000; Vector BA9400) as the anti-BrdU secondary antibody or biotinylated horse anti-goat IgG (1:1000; Vector BA9500) as the anti-DCX secondary antibody, or biotinylated horse anti-mouse IgG (1:1000; Vector BA2000) as the calbindin D-28K secondary antibody, followed by incubation with an ABC Vectastain Kit (Vector). Antigen detection was performed with 0.06% 3,3'-diaminobenzidine (DAB) staining and counterstaining with Nuclear Fast Red (Vector).

For immunofluorescence staining, sections were blocked in 10% equine serum and incubated overnight at 4°C with polyclonal rabbit anti-β-galactosidase (1:2000, MP, 55976) and either polyclonal goat anti-DCX (1:500; Santa Cruz SC8066), monoclonal mouse anti-calretinin (1:3000; Millipore, MAB 1568), monoclonal mouse anti-NeuN (1:500; Millipore, MAB377), or monoclonal mouse anti-calbindin D-28K (1:3000; Sigma Aldrich, C9848). Sections were then incubated for 60 min with a secondary antibody conjugated with AlexaFluor 488 or AlexaFluor 555 (Molecular Probes).

Quantification of BrdU-labeled cells, DCX-positive cells, and calbindin-IR

For BrdU-labeled cell quantification, a modified unbiased stereological procedure was used as previously described (Segi-Nishida et al., 2008). Sections were coded to ensure that the analysis was performed by a blind observer using a light microscope (Nikon Ecripse E200, Tokyo, Japan), BrdU-labeled cells in the SGZ of the hippocampus were counted when they were touching or in the SGZ. Every sixth 30-μm-thick section was evaluated throughout the hippocampus, and the sum of the cell counts was multiplied by six to provide an estimate of the total number of BrdU-labeled cells in the entire region. For DCX-positive cell quantification, 3–4 sections of the DG were photographed using a Biozero BZ-8000 microscope (Keyence Corporation, Osaka, Japan) that was fitted with a 20X objective. The boundaries of the DG were set as regions of interest (ROIs), and each ROI was measured; then, DCX-positive cells were manually counted within the ROI and their number was expressed as the number of cells per square millimeter. For quantification of calbindin-IR, 2 sections of the DG were photographed in the manner described above. The pictures were converted into 16-bit gray scale ones and the average signal intensity of calbindin-IR in the GCL or ML region was quantified by computer-assisted image analysis (ImageJ, NIH, Bethesda, Maryland).

***In situ* hybridization**

In situ hybridization was performed using a DIG-labeled riboprobe as previously

described (Segi-Nishida et al., 2013). A *Ht4r* cDNA template probe was cloned by PCR with gene-specific primers (forward; 5'-ggtcaacaagccctatgctatc-3', reverse; 5'-taagtatcactgggctgag-3', Product Length; 606 bp), verified by sequencing, and used to produce a DIG-labeled riboprobe with the DIG RNA Labeling Kit (Roche, Mannheim, Germany). Coronal brain sections (thickness, 10 μm) were cut on a cryostat, mounted onto slide glasses, fixed in 4% PFA, acetylated, and dehydrated prior to hybridization. Sections were hybridized with the DIG-labeled riboprobe and visualized using an AP-conjugated anti-DIG antibody and BM purple substrate (Roche).

Quantitative real-time PCR

Total RNA was extracted from the DG using the ReliaPrep RNA Miniprep System (Promega), and subjected to reverse transcription with Superscript VILO (Invitrogen), and followed by real-time PCR on a LightCycler (Roche) using the Fast Start DNA Master SYBR Green I (Roche). Expression levels of target genes were normalized to the levels of 18S rRNA. Primer sequences are shown in Table 1. The specificity of each primer set was confirmed by checking the product size by gel electrophoresis.

Statistical Analyses

All data are presented as means ± SEM, and experiments with 2 groups were compared using unpaired Student's *t*-test, whereas experiments with 4 groups were subjected to two-way ANOVA, followed by the Bonferonni *post hoc* test. Significance marks in figures are based on results from the *t*-test and Bonferonni *post hoc* tests. The threshold for statistical significance was $p < 0.05$. All analyses were performed using PRISM 5 software (GraphPad, San Diego, CA).

Table 1. Primer sequences used for real-time RT-PCR.

Gene	Forward	Reverse
Calb1	5'- tctggcttcatttcgacgctg-3'	5'- acaaaggatttcatttccggtga-3'
Tdo2	5'- atgagtgggtgcccgtttg-3'	5'- ggctctgtttacaccagtttgag-3'
Dsp	5'- gctgaagaacactctagccca-3'	5'- actgctgtttcctctgagaca-3'
Il1r1	5'- gtgctactggggctcatttgt-3'	5'- ggagtaagaggacacttgcgaat-3‘
Fos	5'- ctgtcaacacacaggactttt-3'	5'- aggagatagctgctctactttg-3‘
Gadd45b	5'- gttctgctgcgacaatgaca-3'	5'- ttggcttttccaggaatctg-3‘
Nr4a1	5'- gagttcggcaagcctaccat-3'	5'- gtgtacccgtccatgaaggtg-3‘
Arc	5'- agcgggacctgtaccagac-3'	5'- agctgctccagggtcttg-3‘
Egr1	5'- tatgagcacctgaccacagag-3'	5'- gctgggataactcgtctcca-3‘
Bdnf	5'- gacaaggcaacttggcctac-3'	5'- actgtcacacacgctcagctc-3'
Npy	5'- ccacgatgctaggtaaca-3'	5'- ggaaaagtcgggagaac-3'
18S rRNA	5'- gaggccctgtaattggaatgag-3'	5'- gcagcaactttaatatacgctattgg-3'

ACKNOWLEDGEMENTS

I would like to appreciate gratefully to Professor Kazuhisa Nakayama, Graduate School of Pharmaceutical Sciences, Kyoto University and Associate Professor Eri Segi-Nishida, Graduate School of Pharmaceutical Sciences, Kyoto University for their supports through the course of this work.

I would like to express my gratitude to Professor Hidenori Suzuki and Associate Professor Katsunori Kobayashi, Graduate School of Medicin, Nippon Medical School for electrophysiological analysis and helpful discussion.

I would like to express my appreciation to Dr. Shuji Kaneko, Dr. Takayuki Nakagawa, Dr. Kazuki Nagayasu, Mr. Naoya Nishitani Graduate School of Pharmaceutical Sciences, Kyoto University for assays of monoamine measurements and helpful discussion.

I would like to thank Dr. Yukihiko Sugimoto, Dr. Yasushi Okuno, Dr. Hye-Won Shin, Dr. Yohei Katoh, Dr. Hiroyuki Takatsu, Dr. Senye Takahashi, Dr. Kazushi Morimoto, Dr. Tomoaki Inazumi, Ms. Mamiko Sukeno, Ms. Mari Sakaida, Mr. Toshihiko Kira, for their technical advice and helpful discussion.

I also thank members of the Department of Physiological Chemistry, Graduate School of Pharmaceutical Sciences, Kyoto University for their continuous encouragements, helpful discussions and technical supports.

Finally, I would like to thank my family for persistent understanding and support for many things.

REFERENCES

Airan, R. D., Meltzer, L. A., Roy, M., Gong, Y., Chen, H., and Deisseroth, K. (2007). High-speed imaging reveals neurophysiological links to behavior in an animal model of depression. Science *317*, 819-823.

Ambrogini, P., Lattanzi, D., Ciuffoli, S., Agostini, D., Bertini, L., Stocchi, V., Santi, S., and Cuppini, R. (2004). Morpho-functional characterization of neuronal cells at different stages of maturation in granule cell layer of adult rat dentate gyrus. Brain Res. *1017*, 21-31.

Brandt, M. D., Jessberger, S., Steiner, B., Kronenberg, G., Reuter, K., Bick-Sander, A., von der Behrens, W., and Kempermann, G. (2003). Transient calretinin expression defines early postmitotic step of neuronal differentiation in adult hippocampal neurogenesis of mice. Mol Cell Neurosci. *24*, 603-613.

Caccia, S., Fracasso, C., Garattini, S., Guiso, G., and Sarati, S. (1992). Effects of short- and long-term administration of fluoxetine on the monoamine content of rat brain. Neuropharmacology *31*:343-347.

Coghlan, S., Horder, J., Inkster, B., Mendez, M. A., Murphy, D. G., and Nutt, D. J. (2012). GABA system dysfunction in autism and related disorders: from synapse to symptoms. Neurosci. Biobehav. Rev. *36*, 2044-2055.

Conductier, G., Dusticier, N., Lucas, G., Cote, F., Debonnel, G., Daszuta, A., Dumuis, A., Nieoullon, A., Hen, R., Bockaert, J., and Compan, V. (2006). Adaptive changes in serotonin neurons of the raphe nuclei in 5-HT(4) receptor knock-out mouse. Eur. J. Neurosci. *24*:1053-1062.

David, D. J., Samuels, B. A., Rainer, Q., Wang, J. W., Marsteller, D., Mendez, I., Drew, M., Craig, D. A., Guiard, B. P., Guilloux, J. P., Artymyshyn, R. P., Gardier, A. M., Gerald, C., Antonijevic, I. A., Leonardo, E. D., and Hen, R. (2009). Neurogenesis-dependent and -independent effects of fluoxetine in an animal model of anxiety/depression. Neuron *62*:479-493.

Davis, S., Vanhoutte, P., Pages, C., Caboche, J., and Laroche, S. (2000). The MAPK/ERK cascade targets both Elk-1 and cAMP response element-binding protein to control long-term potentiation-dependent gene expression in the dentate gyrus in vivo. J. Neurosci. *20*, 4563-4572.

Decarolis, N. A., and Eisch, A. J. (2010). Hippocampal neurogenesis as a target for the treatment of mental illness: A critical evaluation. Neuropharmacology *58*:884-893.

Decressac, M., Wright, B., David, B., Tyers, P., Jaber, M., Barker, R. A., and Gaillard,

A. (2011). Exogenous neuropeptide Y promotes in vivo hippocampal neurogenesis. Hippocampus *21*:233-238.

Duan, X., Kang, E., Liu, C. Y., Ming, G. L., and Song, H. (2008). Development of neural stem cell in the adult brain. Curr. Opin. Neurobiol. *18*, 108-115.

Duman, R. S., and Aghajanian, G. K. (2012). Synaptic dysfunction in depression: potential therapeutic targets. Science *338*:68-72.

Eisch, A. J., and Petrik, D. (2012). Depression and hippocampal neurogenesis: A road to remission? Science *338*:72-75.

Franklin, K. B. J. and Paxinos, G. (2008). The mouse brain in stereotaxic coordinates. 3rd edition, San Diego: Elsevier Academic Press.

Ge, S., Goh, E. L., Sailor, K. A., Kitabatake, Y., Ming, G. L., and Song, H. (2006). GABA regulates synaptic integration of newly generated neurons in the adult brain. Nature *439*, 589-593.

Ge, S., Yang, C. H., Hsu, K. S., Ming, G. L., and Song, H. (2007). A critical period for enhanced synaptic plasticity in newly generated neurons of the adult brain. Neuron *54*, 559-566.

Gonzalez-Burgos, G., Fish, K. N., and Lewis, D. A. (2011). GABA neuron alterations, cortical circuit dysfunction and cognitive deficits in schizophrenia. Neural Plast. *2011*, 723184.

Holm, M. M., Nieto-Gonzalez, J. L., Vardya, I., Henningsen, K., Jayatissa, M. N., Wiborg, O., and Jensen, K. (2011). Hippocampal GABAergic dysfunction in a rat chronic mild stress model of depression. Hippocampus *21*, 422-433.

Hsieh, T. F., Simler, S., Vergnes, M., Gass, P., Marescaux, C., Wiegand, S. J., Zimmermann, M., and Herdegen, T. (1998). BDNF restores the expression of Jun and Fos inducible transcription factors in the rat brain following repetitive electroconvulsive seizures. Exp. Neurol. *149*, 161-174.

Jessberger, S., and Kempermann, G. (2003). Adult-born hippocampal neurons mature into activity-dependent responsiveness. Eur. J. Neurosci. *18*, 2707-2712.

Kehrer, C., Maziashvili, N., Dugladze, T., and Gloveli, T. (2008). Altered Excitatory-Inhibitory Balance in the NMDA-Hypofunction Model of Schizophrenia. Front. Mol. Neurosci. *1*, 6.

Kobayashi, K., and Suzuki, H. (2007). Dopamine selectively potentiates hippocampal mossy fiber to CA3 synaptic transmission. Neuropharmacology *52*, 552-561.

Kobayashi, K., Ikeda, Y., Sakai, A., Yamasaki, N., Haneda, E., Miyakawa, T., and Suzuki, H. (2010). Reversal of hippocampal neuronal maturation by serotonergic antidepressants. Proc. Natl. Acad. Sci. U S A *107*, 8434-8439.

Kobayashi, K., Ikeda, Y., and Suzuki, H. (2011). Behavioral destabilization induced by

the selective serotonin reuptake inhibitor fluoxetine. Mol. Brain *4*, 12.

Kobayashi, K., Ikeda, Y., Asada, M., Inagaki, H., Kawada, T., and Suzuki, H. (2013). Corticosterone facilitates fluoxetine-induced neuronal plasticity in the hippocampus. PLoS One *8*, e63662.

Ma, D. K., Jang, M. H., Guo, J. U., Kitabatake, Y., Chang, M. L., Pow-Anpongkul, N., Flavell, R. A., Lu, B., Ming, G. L., and Song, H. (2009). Neuronal activity-induced Gadd45b promotes epigenetic DNA demethylation and adult neurogenesis. Science *323*, 1074-1077.

Malberg, J. E., Eisch, A. J., Nestler, E. J., and Duman, R. S. (2000). Chronic antidepressant treatment increases neurogenesis in adult rat hippocampus. J. Neurosci. *20*:9104-9110.

Marin-Burgin, A., Mongiat, L. A., Pardi, M. B., and Schinder, A. F. (2012). Unique processing during a period of high excitation/inhibition balance in adult-born neurons. Science *335*, 1238-1242.

Mendez-David, I., David, D. J., Darcet, F., Wu, M. V., Kerdine-Romer, S., Gardier, A. M., and Hen, R. (2014). Rapid anxiolytic effects of a 5-HT(4) receptor agonist are mediated by a neurogenesis-independent mechanism. Neuropsychopharmacology *39*:1366-1378.

Ming, G. L., and Song, H. (2011). Adult neurogenesis in the Mammalian brain: significant answers and significant questions. Neuron *70*:687-702.

Morinobu, S., Strausbaugh, H., Terwilliger, R., and Duman, R. S. (1997). Regulation of c-Fos and NGF1-A by antidepressant treatments. Synapse *25*:313-320.

Nagayasu, K., Yatani, Y., Kitaichi, M., Kitagawa, Y., Shirakawa, H., Nakagawa, T., and Kaneko, S. (2010). Utility of organotypic raphe slice cultures to investigate the effects of sustained exposure to selective 5-HT reuptake inhibitors on 5-HT release. Br. J. Pharmacol. *161*:1527-1541.

Nakagawa, S., Kim, J. E., Lee, R., Chen, J., Fujioka, T., Malberg, J., Tsuji, S., and Duman R. S. (2002). Localization of phosphorylated cAMP response element-binding protein in immature neurons of adult hippocampus. J. Neurosci. *22*:9868-9876.

Navailles, S., Hof, P. R., and Schmauss, C. (2008). Antidepressant drug-induced stimulation of mouse hippocampal neurogenesis is age-dependent and altered by early life stress. J. Comp. Neurol. *509*:372-381.

Nibuya, M., Morinobu, S., and Duman, R. S. (1995). Regulation of BDNF and trkB mRNA in rat brain by chronic electroconvulsive seizure and antidepressant drug treatments. J. Neurosci. *15*:7539-7547.

Nibuya, M., Nestler, E. J., and Duman R. S. (1996). Chronic antidepressant

administration increases the expression of cAMP response element binding protein (CREB) in rat hippocampus. J. Neurosci. *16*, 2365-2372.

Ninkovic, J., Mori, T., and Gotz, M. (2007). Distinct modes of neuron addition in adult mouse neurogenesis. J. Neurosci. *27*:10906-10911.

Ohira, K., Kobayashi, K., Toyama, K., Nakamura, H. K., Shoji, H., Takao, K., Takeuchi, R., Yamaguchi, S., Kataoka, M., Otsuka, S., Takahashi, M., and Miyakawa, T. (2013). Synaptosomal-associated protein 25 mutation induces immaturity of the dentate granule cells of adult mice. Mol Brain *6*, 12.

Overstreet-Wadiche, L. S., Bromberg, D. A., Bensen, A. L., and Westbrook, G. L. (2006). Seizures accelerate functional integration of adult-generated granule cells. J. Neurosci. *26*, 4095-4103.

Piatti, V. C., Davies, Sala, M. G., Esposito, M. S., Mongiat, L. A., Trinchero, M. F., and Schinder, A. F. (2011). The timing for neuronal maturation in the adult hippocampus is modulated by local network activity. J. Neurosci. *31*, 7715-7728.

Pinnock, S. B., Blake, A. M., Platt, N. J., and Herbert, J. (2010). The roles of BDNF, pCREB and Wnt3a in the latent period preceding activation of progenitor cell mitosis in the adult dentate gyrus by fluoxetine. PLoS One *5*:e13652.

Poeggel, G., Helmeke, C., Abraham, A., Schwabe, T., Friedrich, P., and Braun, K. (2003). Juvenile emotional experience alters synaptic composition in the rodent cortex, hippocampus, and lateral amygdala. Proc. Natl. Acad. Sci. U S A *100*, 16137-16142.

Leranth, C., and Hajszan, T.. (2007). Extrinsic afferent systems to the dentate gyrus. Prog. Brain Res. *163*:63-84.

Li, Y., Luikart, B. W., Birnbaum, S., Chen, J., Kwon, C. H., Kernie, S. G., Bassel-Duby, R., and Parada, L. F. (2008). TrkB regulates hippocampal neurogenesis and governs sensitivity to antidepressive treatment. Neuron *59*:399-412.

Lucas, G., Rymar, V. V., Du, J., Mnie-Filali, O., Bisgaard, C., Manta, S., Lambas-Senas, L., Wiborg, O., Haddjeri, N., Pineyro, G., Sadikot, A. F., and Debonnel, G. (2007). Serotonin(4) (5-HT(4)) receptor agonists are putative antidepressants with a rapid onset of action. Neuron *55*:712-725.

Scharfman, H., Goodman, J., Macleod, A., Phani, S., Antonelli, C., and Croll, S. (2005). Increased neurogenesis and the ectopic granule cells after intrahippocampal BDNF infusion in adult rats. Exp. Neurol. *192*:348-356.

Schmidt-Hieber, C., Jonas, P., and Bischofberger, J. (2004). Enhanced synaptic plasticity in newly generated granule cells of the adult hippocampus. Nature *429*, 184-187.

Segi-Nishida, E., Warner-Schmidt, J. L., and Duman, R. S. (2008). Electroconvulsive seizure and VEGF increase the proliferation of neural stem-like cells in rat hippocampus. Proc. Natl. Acad. Sci. U S A *105*:11352-11357.

Segi-Nishida, E., Sukeno, M., Imoto, Y., Kira, T., Sakaida, M., Tsuchiya, S., Sugimoto, Y., and Okuno, Y. (2013). Electroconvulsive seizures activate anorexigenic signals in the ventromedial nuclei of the hypothalamus. Neuropharmacology *71*:164-173.

Seress, L., Abraham, H., Paleszter, M., and Gallyas, F. (2001). Granule cells are the main source of excitatory input to a subpopulation of GABAergic hippocampal neurons as revealed by electron microscopic double staining for zinc histochemistry and parvalbumin immunocytochemistry. Exp. Brain Res. *136*:456-462.

Shin, R., Kobayashi, K., Hagihara, H., Kogan, J. H., Miyake, S., Tajinda, K., Walton, N. M., Gross, A. K., Heusner, C. L., Chen, Q., Tamura, K., Miyakawa, T., and Matsumoto, M.. (2013). The immature dentate gyrus represents a shared phenotype of mouse models of epilepsy and psychiatric disease. Bipolar Disord. *15*, 405-421.

Sillaber, I., Panhuysen, M., Henniger, M. S., Ohl, F., Kuhne, C., Putz, B., Pohl, T., Deussing, J. M., Paez-Pereda, M., and Holsboer, F. (2008). Profiling of behavioral changes and hippocampal gene expression in mice chronically treated with the SSRI paroxetine. Psychopharmacology (Berl) *200*:557-572.

Song, J., Zhong, C., Bonaguidi, M. A., Sun, G. J., Hsu, D., Gu, Y., Meletis, K., Huang, Z. J., Ge, S., Enikolopov, G., Deisseroth, K., Luscher, B., Christian, K. M., Ming, G. L., and Song, H. (202). Neuronal circuitry mechanism regulating adult quiescent neural stem-cell fate decision. Nature *489*:150-154.

Song, J., Sun, J., Moss, J., Wen, Z., Sun, G. J., Hsu, D., Zhong, C., Davoudi, H., Christian, K. M., Toni, N., Ming, G. L., and Song, H. (2013). Parvalbumin interneurons mediate neuronal circuitry-neurogenesis coupling in the adult hippocampus. Nat. Neurosci. *16*:1728-1730.

Stewart, C. A., and Reid, I. C. (1994). Ketamine prevents ECS-induced synaptic enhancement in rat hippocampus. Neurosci. Lett. *178*, 11-14.

Takao, K., Kobayashi, K., Hagihara, H., Ohira, K., Shoji, H., Hattori, S., Koshimizu, H., Umemori, J., Toyama, K., Nakamura, H. K., Kuroiwa, M., Maeda, J., Atsuzawa, K., Esaki, K., Yamaguchi, S., Furuya, S., Takagi, T., Walton, N. M., Hayashi, N., Suzuki, H., Higuchi, M., Usuda, N., Suhara, T., Nishi, A., Matsumoto, M., Ishii, S., and Miyakawa, T. (2013). Deficiency of Schnurri-2, an MHC enhancer binding protein, induces mild chronic inflammation in the brain and confers

molecular, neuronal, and behavioral phenotypes related to schizophrenia. Neuropsychopharmacology *38*, 1409-1425.

Tanaka, K. F., Samuels, B. A., and Hen, R. (2012). Serotonin receptor expression along the dorsal-ventral axis of mouse hippocampus. Philos. Trans. R. Soc. Lond. B. Biol. Sci. *367*:2395-2401.

Tanis, K. Q., Duman, R. S., and Newton, S. S. (2008). CREB binding and activity in brain: regional specificity and induction by electroconvulsive seizure. Biol. Psychiatry *63*, 710-720.

Tashiro, A., Sandler, V. M., Toni, N., Zhao, C., and Gage, F. H. (2006). NMDA-receptor-mediated, cell-specific integration of new neurons in adult dentate gyrus. Nature *442*, 929-933.

Thome, J., Sakai, N., Shin, K., Steffen, C., Zhang, Y. J., Impey, S., Storm, D., and Duman, R. S. (2000). cAMP response element-mediated gene transcription is upregulated by chronic antidepressant treatment. J. Neurosci. *20*, 4030-4036.

Tonder, N., Kragh, J., Bolwig, T., and Zimmer, J. (1994). Transient decrease in calbindin immunoreactivity of the rat fascia dentata granule cells after repeated electroconvulsive shocks. Hippocampus *4*, 79-83.

Walton, N. M., Zhou, Y., Kogan, J. H., Shin, R., Webster, M., Gross, A. K., Heusner, C. L., Chen, Q., Miyake, S., Tajinda, K., Tamura, K., Miyakawa, T., and Matsumoto, M. (2012). Detection of an immature dentate gyrus feature in human schizophrenia/bipolar patients. Transl. Psychiatry *2*, e135.

Warner-Schmidt, J. L., Flajolet, M., Maller, A., Chen, E. Y., Qi, H., Svenningsson, P., and Greengard, P. (2009). Role of p11 in cellular and behavioral effects of 5-HT4 receptor stimulation. J. Neurosci. *29*:1937-1946.

Wu, X., and Castren, E. (2009). Co-treatment with diazepam prevents the effects of fluoxetine on the proliferation and survival of hippocampal dentate granule cells. Biol. Psychiatry *66*:5-8.

Yamasaki, N., Maekawa, M., Kobayashi, K., Kajii, Y., Maeda, J., Soma, M., Takao, K., Tanda, K., Ohira, K., Toyama, K., Kanzaki, K., Fukunaga, K., Sudo, Y., Ichinose, H., Ikeda, M., Iwata, N., Ozaki, N., Suzuki, H., Higuchi, M., Suhara, T., Yuasa, S., and Miyakawa, T. (2008). Alpha-CaMKII deficiency causes immature dentate gyrus, a novel candidate endophenotype of psychiatric disorders. Mol. Brain *1*, 6.

Zhao, C., Deng, W., and Gage, F. H. (2008). Mechanisms and functional implications of adult neurogenesis. Cell *132*, 645-660.

Zhao, C., Warner-Schmidt, J., Duman, R. S., and Gage, F. H. (2012). Electroconvulsive seizure promotes spine maturation in newborn dentate granule cells in adult rat.

Dev. Neurobiol. *72*, 937-942.